A

"The Microflown, a particle velocity sensor"

In this part the specifics of the Microflown will be discussed. It starts with a rather theoretical paragraph in which the analytical model is presented that describes the physical processes that govern the behaviour of the Microflown. The emphasis will be on the frequency dependent behaviour more than the low frequency sensitivity. In chapter 1 and 2 the way that the Microflown operates is explained in a more practical way.

The model predicts the frequency dependent behaviour of the Microflown. It will be shown that there are two corner frequencies, one is caused by the heat capacity of the sensors and the other is due to diffusion effects. The model predicts a flat frequency response for low frequencies, a -6dB/oct roll-of at about 500Hz-1kHz due to diffusion effects and an additional -6dB/oct roll-of at about 2-15kHz as result of the thermal mass of the sensors.

However DC (steady) flow sensors are commonly known, and the Microflown is in fact nothing more than such a flow sensor, it is still difficult to model the (very) low frequency behaviour of the Microflown. Much effort is spent on this subject so in the near future this model should be available.

Another very important effect is the so-called package gain. Due to proper packaging the output of a Microflown will rise dramatically. This has a positive effect on the noise properties. The effect itself is not yet studied very well. However measurements show that the sensitivity improvement is about 3 to 30 times and that it is only slightly frequency dependent. The subject is treated in paragraph A2.

The half-inch ICP probe is made for measurement purposes. The aim was to construct a device that showed a resemblance to the sound pressure probe that is used mostly: the half-inch microphone. The preamplifier is made in such way that the output is compatible to the ICP standard: it is a two-wire system where 4mA current is used as powering and the output voltage is used as readout. This way of powering is become established over the last years. In part A3 the specifics of this probe can be found.

For a lot of applications (like e.g. array techniques, acoustic holography and multi-dimensional sound intensity determination) the similarity in the acoustic response is an important issue. In paragraph A4 some results are presented.

The most important concern of an instrument used for measurement purposes is the ability to calibrate it in a relative simple manner. It was the first question that was raised after the invention of the Microflown. A lot of possible methods where tried out and the best three are explained in paragraph A5.

In the last decades a lot of different types of microphones are manufactured for a lot of different applications. The similarities and differences of these microphones and Microflowns are treated in paragraph A6.

A1 MODEL OF THE MICROFLOWN

In this chapter an analytical model is presented that describes the physical processes that govern the behaviour of the Microflown and determines its sensitivity. The emphasis will be on the frequency dependent behaviour more than the low frequency behaviour.

The Microflown that is considered in this chapter consists of two heaters that act simultaneously as sensors, and the temperature distribution around these heaters is described. Due to forced convection by an acoustic wave (i.e. the particle velocity), a small correction to this temperature profile is added, and a temperature difference between the two sensors occurs. This temperature difference, which is proportional to the sensitivity, is calculated with perturbation theory. Consequently the frequency dependent behaviour of the sensitivity can be analysed; it seems that there are two important corner frequencies, the first related to the velocity of heat diffusion between the sensors, the second related to the heat capacity of the heaters.

In [1] a reliable and solid description is given for the realisation of the Microflown in a channel, i.e. with both heaters between fixed walls around it. Here, a model is presented that describes a situation without walls above and under it. This theory is compared to experimental results. The chapter is based on the work of Joost van Honschoten who is a PhD student at the University of Twente. Much work is also be done by two Russian scientists V.B. Svetovoy and I.A. Winter. Their work [1,2] is greatly acknowledged.

Modelling the temperature distribution

In the following paragraph a model is developed in which the Microflown consist of two long heaters of width $2L$ and negligible height, separated by a distance a, with a much larger than L.

These heated wires cause a temperature distribution of the air around them. This undisturbed temperature profile, not yet influenced by an acoustical wave, is calculated.

Model

This will be used as a starting point for calculating of the temperature difference of the heaters that occurs when a flow is applied, by adding a perturbation to the original temperature profile.

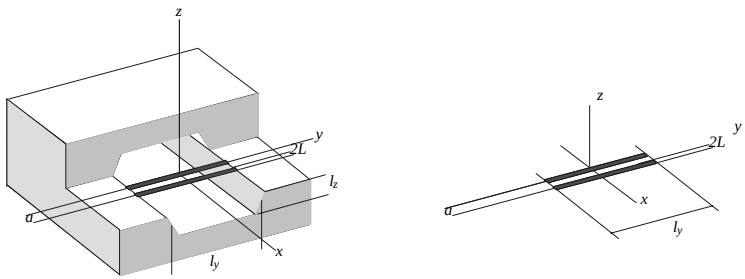

Fig. 1: Geometry of the sensor used in the analysis. left: geometry used in model of [1]; right: this model, without walls above and under the heaters.

In former days the Microflown was designed similar to a mass flow sensor. Such sensors operate with a heater and two temperature sensors around it. These sensors where called the SHS type of Microflowns referring to the sensor-heater-sensor configurations. Nowadays the Microflown consists only of two heated temperature sensors. This configuration is called the SS or TSM. The first is referring to the physical configuration and the latter to two-sensor-Microflown.

The temperature sensors of the Microflown are implemented as platinum resistors and are powered by an electrical current dissipating an electrical power causing it to heat-up. An increase of the temperature of the sensors leads to an increase of the resistance as well. If no particle velocity is present the sensors will have a typical operational temperature of about 200ºC to 400ºC and all the heat is transferred in the surrounding air. When particle velocity is present, it asymmetrically alters the temperature distribution around the resistors. The temperature difference of the two sensors quantifies the particle velocity.

The stationary situation

The temperature profile around the heaters in the two sensor-realisation of the Microflown is adequately described in [1] for the configuration of the channel with fixed walls in the positive and negative

z-direction. See Fig. 1. A good starting point to describe the temperature change due to a sound wave by perturbation analysis is shown to be the temperature distribution in which the fluid (i.c. the air) is in rest. The sensitivity of the Microflown is deduced from the temperature difference between the sensors/heaters. In [1] both unperturbed and perturbed temperature profiles are written as a Fourier series, an expansion in harmonics. Here the temperature distribution for the two free wires (Fig. 1 right is presented as an analytical expression).

Starting with the stationary heat transport equation

$$\nabla(k\nabla T) = Q \tag{55}$$

where $k=k(T)$ represents the heat conductivity of the air, and Q is the amount of heat of the heater per unit of time and volume.

Suppose a heater of infinite length in the y-direction (l_y much larger than other dimensions), of width $2L$ in the x-direction and negligible height in the z-direction. After this analysis, it can be checked if the assumptions of a very large l_y and an infinitely thin heater were justified.

Since the total power is P, and the power per unit of length is P/l_y for Q can be written:

$$Q = \frac{P}{2l_y L} F(x)\delta(z) \tag{56}$$

where $F(x) = 0 \;\; for \; |x| > L \; and \; F(x) = 1 \;\; for \; |x| < L$

Assuming that k is almost independent of T, the differential equation for the temperature in the channel reads:

$$(\partial_x^2 + \partial_z^2)T = -\frac{P}{2l_y kL} F(x)\delta(z) \tag{57}$$

Since the length l_y is taken large and the temperature along this direction is assumed to be constant, the problem is reduced to two dimensions, in contrast to the model based on the expansion in harmonics as presented in [1].

To solve this differential equation, the analogue with electrostatic theory may be used. There are different ways to solve the equation and one is described here. Assume an infinitely long wire (along the y-axis)

of uniform charge density in *C/m*, the analogue of the infinitely long heater of uniform temperature.

The three-dimensional Poisson equation for a point charge leads to a Coulomb potential of the form $1/r$. In two dimensions the potential behaves as $ln(r)$, having logarithmic singularities at both ends $r \to 0$ and $r \to \infty$. Of course the solution for T should go to a finite temperature at infinity. However, as a consequence of the two dimensions there is no such solution. Physically, the problem is actually three-dimensional; the two-dimensional approximation can only be applied when all the interesting distances are much smaller than l_y. Therefore, a physical cut-off parameter $\varepsilon \sim 1/l_y$ could be introduced. The boundary condition (the case $T \to 0$, which can always be shifted to a constant since the original heat equation includes only differentials of the temperature) has to be fulfilled approximately somewhere at $r \sim l_y$.

Considering a very narrow, infinitely long heater, the differential equation for the temperature in the channel would be:

$$(\partial_x^2 + \partial_z^2)T = -\frac{P}{l_y k}\delta(x)\delta(z) \tag{58}$$

The difference with Eq. 57 is that $F(x)/2L$ has been changed into $\delta(x)$, which is justified for a very narrow heater. The right hand side is nonzero only in the origin.

Using the analogue situation of the potential V of an infinitely long and narrow charged wire (with charge density λ [C/m]), where

$$V(r) = V\left(\sqrt{x^2 + z^2}\right) = -\frac{\lambda}{2\pi\varepsilon_0}\ln\sqrt{x^2 + z^2} \tag{59}$$

it is seen that the solution of Eq. 58 is:

$$T(x,z) = A\ln\left(\sqrt{x^2 + z^2}\right) \; with \; A = \frac{-P}{2\pi k l_y} \tag{60}$$

The argument of the logarithm has dimension 'meters' and it should be made dimensionless. Since l_y is the parameter with the proper dimension, one can write

$$T(x,z) = \frac{-P}{2\pi k l_y} \ln\left(\frac{r}{l_y}\right) \tag{61}$$

Only some constant should be added. If this temperature profile is assumed, the temperature is zero on the circle $r=l_y$, so formally r should not exceed this (relatively) large value. The temperature is singular at the origin, as it should be for a point source. However, this property is not realistic since the heater temperature is a known quantity. To avoid this problem the heater with finite width, $2L$, is considered. A point source (i.e. an infinitely thin and long wire) is placed in every point of such a heater and subsequently the average value of the potential is taken to obtain

$$T(x,z) = \frac{-P}{2\pi k l_y} \frac{1}{2L} \int_{-L}^{L} \ln \frac{\sqrt{(x-x')^2 + z^2}}{l_y} dx' \tag{62}$$

Evaluating the temperature in $(x,z)=(0,0)$ yields

$$T(0,0) = \frac{-P}{2\pi k l_y} \left(\ln\left(L / l_y\right) - 1\right) \tag{63}$$

and the temperature is zero far from the heater in a distance $\sim l_y$.

This temperature distribution is taken as a starting-point to proceed and to consider the influence of the sound wave. However, Eq. 62 is only an approximation, since the cut-off parameter (ε) is not defined very strictly. Instead of l_y one could take $2l_y$ or choose any other coefficient of the order of 1. That means that the approximation is good if $-\ln(L/l_y) >> 1$. (For practical usage it is not too bad, but a better solution could be constructed by distributing three-dimensional point sources on the stripe $2L \times l_y$, therefore not disregarding the third y-dimension).

It may be obvious that during the calculation of the temperature profile above, only one heater was considered, see Eq.57, corresponding to the SHS (sensor-heater-sensor) configuration. The situation of two heaters of width $2L$ and mutual distance $2a$ changes the function F into

$$\begin{cases} F(x) = 1 \;\; for \;\; -L-a < x < L-a; \; F(x) = 1 \;\; for \;\; a-L < x < a+L; \\ F(x) = 0 \;\; else \end{cases} \tag{64}$$

Model

Because of symmetry, Eq. 55 can now be solved for only positive values of x. Since the solution for T will be a sum of the two solutions for which only one source is present, each solution shifted in x-direction, the new solution for T is not fundamentally different from Eq.62. See also [1].

For this T could be taken for example an expression of the form $T_{total}(x)=T_{left\ heater}(x)+T_{right\ heater}(x)$, where $T_{right\ heater}(x)=T(x-a)$ and $T_{left\ heater}(x)=T(x+a)$.

An example of a realistic temperature distribution is shown in Fig. 2 According to the model, the sensors itself do have a temperature of about 580K. Between the sensors the temperature seems to drop about 100K! Regular sound levels (conversation, face-to-face) have sound levels of about 60dB. At these levels the measured temperature difference of the two sensors of the Microflown will vary only ten milli-Degrees Kelvin.

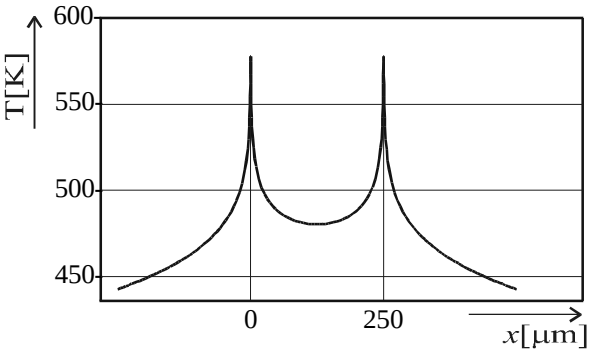

Fig. 2: Temperature distribution around the two sensors in a stationary situation. The heaters are located at $x=0$ and $x=250$ μm, the dissipated power is about 10mW.

Low frequency sensitivity (LFS)

Because the theory to describe the operation principle of the Microflown is rather difficult, in this paragraph the principle is explained in a more practical approach. The following paragraph includes the mathematical description.

A single wire (anemometer) can also be deployed as a velocity sensor, however the underlying principles of anemometer and Microflown

operation are different. To explain the operation of the Microflown, first only one wire is examined.

The anemometer operates due to the convective cooling down of the wire. It operates from 1cm/s upwards (in air) for which Kings law applies (the cooling down is proportional to the square root of the velocity). An anemometer cannot distinguish between positive and negative velocity direction.

For lower air velocities the wire will not cool down and Kings law does not apply. Although the wire does not cool down, due to the convection, the temperature distribution around the hot wire will alter. To calculate this due-to-convection-altered temperature profile, perturbation theory can be used. This theory is explained in the following paragraph.

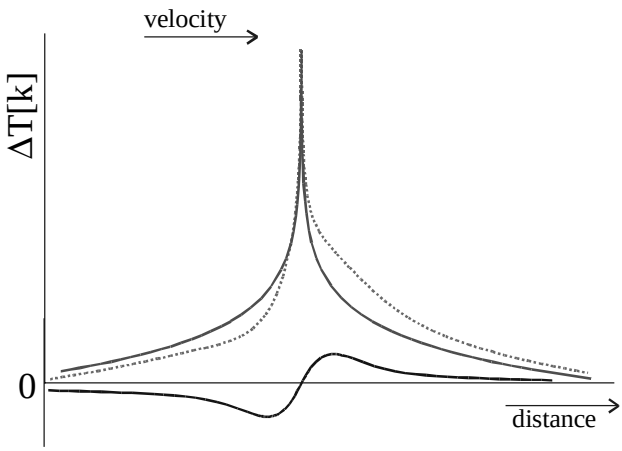

Fig. 3: The temperature distribution around one wire. Solid line: no flow, dotted line: due to convection perturbed temperature profile (the wire itself does not cool down). The lower line is the perturbation due to convection, at the position of the wire the perturbation is zero: the wire will not cool down.

A Microflown consists of two heated wires. It operates in a flow range of 100nm/s up to about 0.1-1m/s. A first order approximation shows no cooling down of the sensors. Particle velocity causes the temperature distribution of both wires to alter and the total temperature distribution causes both wires to differ in temperature; because it is a linear system, the total temperature distribution is simply the sum of the temperature distribution of the two single wires.

Model

Due to the convective heat transfer, the upstream sensor will be heated less by the downstream sensor and vice versa. Due to this operation principle, the Microflown can distinguish between positive and negative velocity direction.

Two forms of heat transport play a role; heat diffusion and convection (radiation is negligible here). For large sensor spacing, the effects of the (1 dimensional) convective heat transfer (due to particle velocity) is reduced by the (three dimensional) diffusion. In other words, for a large sensor spacing, the convective heat transfer does not reach the other sensor and because of this the temperature of the sensors will not alter (the perturbation is zero for large distance, see Fig. 3).

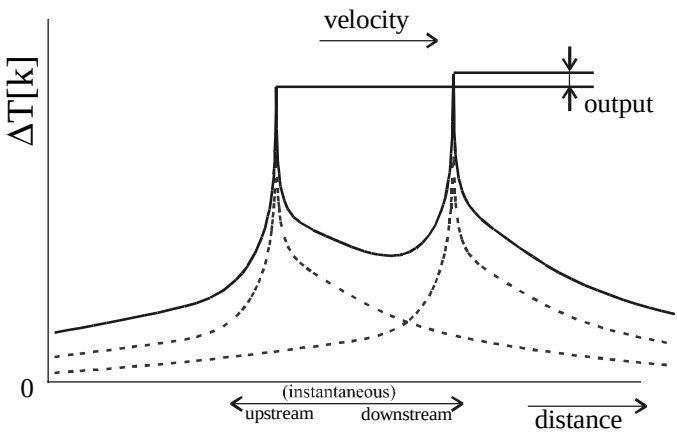

Fig. 4: Dotted line: temperature distribution due to convection for two heaters. Both heaters have the same temperature. Solid line: sum of two single temperature functions: a temperature difference occurs**.**

If the sensors are brought very close to each other, almost no temperature differences are possible since a temperature difference results in a relatively large diffusion heat transfer in the opposite direction.

Influence an acoustical wave on the temperature profile

To get insight into the influence of an acoustical wave on the temperature difference of the sensors, that is related to the final output

signal, in this paragraph the change of the temperature profile due to a small perturbation is calculated. The convection term (i.e. the sound field) involved is assumed to be small.

When an acoustical wave is applied, a particle flow is present in the channel and the temperature distribution should obey the following time-dependent heat transport equation

$$\rho c_p(\partial_t T + v\nabla T) - \nabla(k\nabla T) = Q \tag{65}$$

where $\boldsymbol{v}$ represents the particle velocity, ρ the density and c_p the specific heat capacity of the fluid (i.c. the air). The convection term proportional to $\boldsymbol{v}$ causes the asymmetry of the temperature distribution, leading to a temperature difference of the two sensors. The heat conduction coefficient k is assumed to be not dependent on T, which is justified for lower temperatures (see [1]). This makes Eq. (65) linear in T.

It is assumed that the velocity of the flow is small. Then Eq. (65) can be solved by solving Eq. (1) with a small addition δT, that is proportional to $\boldsymbol{v}$. Taking only terms of first order, the equation for the perturbation δT becomes

$$\partial_t \delta T - D\nabla^2 \delta T = -v\partial_x T \tag{66}$$

where $D = k/\rho c_p$ is the thermal diffusion coefficient of the air, about $1.9\cdot 10^{-5}\, m^2 s^{-1}$. The velocity $\boldsymbol{v}$ is supposed to have only a component in the x-direction.

Now Eq. (66) should be solved, using the boundary conditions $\delta T = 0$ for $x \rightarrow \pm\infty$. If the perturbation δT is taken of the form

$$\delta T = e^{i2\pi f t}\delta T(x, y) \tag{67}$$

the new equation for δT becomes

$$i\,2\pi f \delta T - D(\partial_x^2 + \partial_z^2)\delta T = -v\partial_x T \tag{68}$$

From Eq. (59) follows that

$$\partial_x T = \frac{-P}{2\pi k l_y}\frac{1}{2L}\int_{-L}^{L}\frac{x - x'}{(x - x')^2 + z^2}dx' \tag{69}$$

where the derivation and the integration have been interchanged.

Model

To eliminate the *z*-coordinate, the Fourier transforms $\delta\overline{T}(x,q)$ and $\overline{T}(x,q)$ from respectively $\delta T(x,z)$ and $T(x,z)$. So

$$\delta T(x,z) = \int_{-\infty}^{\infty} \delta\overline{T}(x,q) e^{iqz} dq \tag{70}$$

$$\partial_x T(x,z) = \int_{-\infty}^{\infty} \partial_x \overline{T}(x,q) e^{iqz} dq \tag{71}$$

Substituting these expressions into Eq.(68) yields

$$\delta\overline{T}'' - K^2 \delta\overline{T} = \frac{v}{D} \partial_x \overline{T} \tag{72}$$

where

$$K^2 = q^2 + i\frac{2\pi f}{D} \tag{73}$$

The problem that arises is to find $\partial_x T(x,q)$. It can be found by taking the inverse transform of Eq. (69), i.e.

$$\partial_x \overline{T}(x,q) = \frac{1}{2\pi}\left(-\frac{P}{2\pi k l_y}\frac{1}{2L}\right)\int_{-L}^{L}\int_{-\infty}^{\infty} \frac{x-x'}{(x-x')^2+z^2} e^{-iqz} dz \cdot dx' \tag{74}$$

Using a mathematical handbook [5] these integrals are evaluated as

$$\partial_x \overline{T}(x,q) = -\frac{P}{2\pi k l_y}\frac{1}{2L}\begin{cases} \dfrac{sinh(|q|L)}{|q|} e^{-|q|x} & x > L \\ \dfrac{sinh(|q|x)}{|q|} e^{-|q|L} & 0 < x < L \end{cases} \tag{75}$$

For negative values of *x* the sign of the function changes. With this expression for $\partial_x T(x,q)$, the differential equation for $\delta T(x,q)$, Eq. (72), with boundary conditions $\delta T=0$ for $x \to \pm\infty$ should now be solved. This can be done by solving first the homogeneous equation, and then searching a particular solution. The total solution for $\delta T(x,q)$ then becomes

$$\delta\overline{T} = i\frac{v}{2\pi f}\frac{P}{4\pi k l_y}\left(\frac{\sinh(|q|L)}{|q|L}e^{-|q|x} - \frac{\sinh(KL)}{KL}e^{-Kx}\right) \tag{76}$$

It is written in the range $x>L$, since this is the interval of interest for δT to calculate the correction to the sensor temperature.

When the situation of two heaters (sensors) is considered, the function for T consists of two terms of the form Eq. (10), e.g. $T_{left\ heater}$ and $T_{right.heater}$, each term shifted over a certain distance x, as stated above.

Actually the differential equation for $\delta\overline{T}\ (x,q)$ should then be solved with both terms for $\partial_x T\ (x,q)$. Later on, to calculate the temperature difference of a sensor due to the flow, the expression for $\delta\overline{T}\ (x,q)$ shall have to be averaged over the (x-)width of the heater. In [1] it is shown and proved that the sensitivity of the sensors in the TSM-configuration, is in fact similar to the sensitivity of the SHS-configuration, for which the analyse above applies, when the distance a between heater and sensor in the SHS-situation is the same as the distance between heater and sensor in the TSM-construction.

Concluding, the expression for $\delta\overline{T}\ (x,q)$ in Eq. (76) is sufficient to calculate the temperature difference for the two-sensors-construction.

Finding an analytical form of the Fourier transform of this expression is troublesome because of the first term between brackets. Only a numerical evaluation seems possible. However, it should be realised that the only place of interest of $\delta T\ (x,z)$is at $z=0$.The sensor can be at any x but its z-coordinate is always zero.

So, to know the correction to the sensor temperature $\delta T\ (x,0)$ is calculated Eq. (76) is averaged over the sensor width (from $x=-L$ to $x=L$) and then follows

$$\delta T(x,0) = 2i\frac{v}{2\pi f}\frac{P}{4\pi k l_y}\int_0^\infty\left([\frac{\sinh(qL)}{qL}]^2 e^{-qx} - [\frac{\sinh(KL)}{KL}]^2 e^{-Kx}\right)dq \tag{77}$$

Subsequently, the temperature difference of the sensors can be calculated from

$$\Delta T = 2\delta T(a,0) \tag{78}$$

The integral in Eq. (77) can not be evaluated analytically. Nevertheless, it is possible to make the approximation of $L\rightarrow 0$; a

negligible width of the sensors compared to their distance *a*. The squared terms in front of the exponents then go to 1, and using

$$\int_0^\infty e^{-\sqrt{t^2+i\bar{f}}}\,dt = \sqrt{i\bar{f}}\,K_1(\sqrt{i\bar{f}}) \tag{79}$$

with f a dimensionless frequency, and $K_1(x)$ the modified Bessel function of the first kind, one obtains for ΔT

$$\Delta T = \frac{2vP}{4\pi^2 k l_y fa}(1-\sqrt{i\bar{f}}\,K_1(\sqrt{i\bar{f}})) \tag{80}$$

In the expressions above, the frequency is made dimensionless by introducing $\bar{f} = f\,2\pi a^2 D^{-1}$. This corresponds to $\bar{f} = f / f_D$, where $f_D \equiv D / 2\pi a^2$ is determined by the thermal diffusion and forms an important scale factor in the expression (80). The frequency f_D is called the thermal diffusion frequency.

For large f, the term with the Bessel function decreases exponentially, and the real part of ΔT (which is the part of interest) behaves as f^{-1}.

The situation of small f means that $\bar{f} \ll 1$, so $f \ll f_D$. In this situation the behaviour of the Bessel function is as

$$\sqrt{i\bar{f}}\,K_1(\sqrt{i\bar{f}}) = 1 + \frac{i\bar{f}}{2}\ln\frac{\sqrt{i\bar{f}}}{2} + O(\bar{f}). \tag{81}$$

of which the real part is of importance for ΔT. This means that ΔT does not depend on frequency if f is small compared to the thermal frequency f_D,.

For evaluating the first term between brackets of Eq.(76), when the approximation of $L \to 0$ is *not* made, the following approach may be possible. Instead of averaging $\sinh(|q|L)/|q|x \times e^{-|q|x}$ over the sensor width $-L<x<L$, and then integrating over q, one could integrate first over q, and then average the answer over the width x. This leads to

$$\int_0^\infty \frac{\sinh(|q|L)}{|q|x} e^{-|q|x}\,dq = \frac{1}{2L}\ln\frac{x+L}{x-L} \tag{82a}$$

and then

$$\frac{1}{2L}\int_{a-L}^{a+L}\frac{1}{2L}\ln\left(\frac{x+L}{x-L}\right)dx=\frac{1}{4L^2}\left(a\ln\left(1-\left(\frac{2L}{a}\right)^2\right)+2L\ln\left(\frac{a+2L}{a-2L}\right)\right) \quad (82b)$$

For small L, Eq. (82b) becomes equal to a^{-1}, and therefore corresponds to the first term in Eq. (82).

Considering Eq. (79) it can be seen that ΔT is proportional to the dissipated power P (or rather the power per unit length P/l_y), as well as to the velocity v of the acoustic wave.

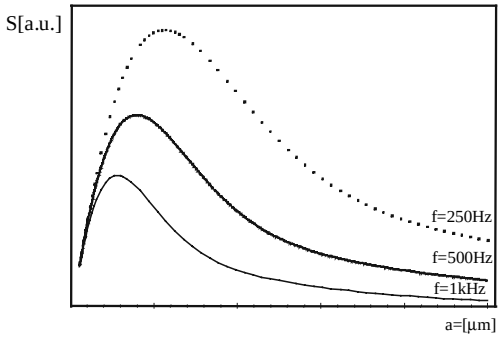

Fig. 5: Sensitivity S(a,f) for f=250Hz (points), 500Hz (dotted) and 1kHz.

From ΔT, the sensitivity S is easily calculated. This sensitivity S is linearly proportional to ΔT and therefore a function of frequency and distance a between the sensors. Consider the form

$$\Delta T(a,f)=\mathrm{Re}\left(const\,\frac{1}{f}\left(\frac{1}{a}-\sqrt{if\frac{2\pi}{D}}K_1\left(a\sqrt{if\frac{2\pi}{D}}\right)\right)\right) \quad (83)$$

In Fig. 5, $\Delta T\ (a,f)$ is seen as a function of a, for different frequencies. In Fig. 6, $\Delta T(f)$ is plotted as a function of f, on a logarithmic scale, where a is now a parameter.

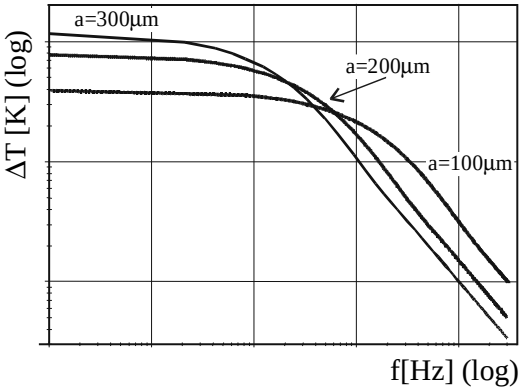

Fig. 6: Output signal $\Delta T(a,f)$, on a logarithmic scale, for $a=100\mu m$, $a=200\mu m$ and $a=300\mu m$.

The effect of the heat capacity of the sensors

The next step in the approach should be to take into consideration the heat capacity of the sensors. The effect of this heat capacity becomes important for increasing frequencies. In Eq. (13) an additional term appears with respect to this effect, so

$$(\rho c_p)_{air}(\partial_t T + \vec{v}\nabla T) - h(\rho c_p)_{Pt}\partial_t T - \nabla(k\nabla T) = Q \tag{84}$$

where h is the thickness of the wire and $(\rho c_p)_{Pt}$ represent the density and heat capacity of this (platinum) sensor. If, again, a small perturbation δT is added to this equation, the same approach as to Eq. (66) leads to

$$\partial_t \delta T - D\nabla^2 \delta T = -v\partial_x T + h\frac{(\rho c_p)_{Pt}}{(\rho c_p)_{air}}\left(F(x-a)\partial_t \delta T + F(x+a)\partial_t \delta T\right) \tag{85}$$

assuming that the two beams of the two-sensor-Microflown are at $x=\pm a$. After the same transformation from $\delta T(x,z)$ to $\delta T(x,q)$, this can be written as

$$\delta\bar{T}''(x,q) - (q^2 + i\tfrac{2\pi f}{D})\nabla^2\delta\bar{T}(x,q) = \frac{v}{D}\partial_x\bar{T}(x,q) - \frac{h}{D}\frac{(\rho c_p)_{Pt}}{(\rho c_p)_{air}}\left(F(x-a)+F(x+a)\right)\partial_t\bar{T}(x,q) \tag{86}$$

and since in the limit for narrow beams $F(x)$ can be approximated by $F(x) = 2L\delta(x)$, the equation becomes

$$\delta\overline{T}''(x,q) - K^2\nabla^2\delta\overline{T}(x,q) = \frac{v}{D}\partial_x\overline{T}(x,q) - 2iLh\frac{2\pi f}{D}\frac{(\rho c_p)_{Pt}}{(\rho c_p)_{air}}\partial_t\overline{T}(a,q) \quad (87)$$

If β is defined here as $\beta = Lh(\rho c_p)_{Pt}/(\rho c_p)_{air}$, this parameter will appear to determine the corner frequency related to the heat capacity of the sensors.

It is not easy to solve the differential equation (87) since it relates $\delta\overline{T}(x,q)$ and its derivatives to the value of $\delta\overline{T}(x,q)$ in $x=a$. But since the point of interest of the solution $\delta\overline{T}(x,q)$ is only $\delta\overline{T}(a,q)$, an expression for $\delta\overline{T}(a,q)$ and therefore for $\delta T(a,z)$ in $z=0$ can be found, by substituting $x=a$ in the equation. Then for ΔT, which equals $2\delta T(a,0)$, is found

$$\Delta T = 2\delta T(a,0) = \frac{1}{1+2i\beta\frac{2\pi f}{D}}Re\left\{\frac{2vP}{4\pi^2 kl_y f}\left(\frac{1}{a} - \sqrt{if\frac{2\pi}{D}}K_1\left(a\sqrt{if\frac{2\pi}{D}}\right)\right)\right\} \quad (88)$$

If Eq. (88) is compared to the former expression for the temperature difference, Eq. (80) it is noticed that because of the heat capacity of the heaters, a factor $\left(1+2i\beta\frac{2\pi f}{D}\right)^{-1}$ appears in front. In terms of frequency dependent transition functions, this factor in front corresponds to a first order transition with corner frequency:

$$f_{heat\ cap} = \frac{D}{4\pi\beta} = \frac{D}{4\pi Lh}\frac{(\rho c_p)_{air}}{(\rho c_p)_{Pt}} \quad (89)$$

Concluding, the first factor in front of Eq. (88) corresponds to a first order transition with a corner frequency determined by the heat capacity of the sensors.

Intermezzo: from model to measurements

The behaviour of the original expression, Eq. (88), looks like, but is not perfectly similar to that of a first order low pass function. For frequencies small compared to the thermal diffusion frequency f_D, the function is constant (independent of f), for frequencies much higher than this frequency the function is inversely proportional to f; see Fig. 6. Nevertheless, there is a large region around the thermal diffusion frequency f_D, for which the function slowly decreases (on a logarithmic

scale): although the thermal frequency is an important scale factor in the expression for ΔT, it does not equal the corner frequency of the first order transition. The sensitivity for steady ('DC-') flow can be found from the expression for ΔT, in which $\lim f \downarrow 0$ is taken. Since:

$$\lim_{f\downarrow 0} \mathrm{Re}\left(\frac{\frac{1}{a}-\sqrt{if}\,K_1(a\sqrt{if})}{f}\right) = \lim_{f\downarrow 0}\left(-\frac{i}{2}\ln\frac{a\sqrt{if}}{2}\right) = \frac{\pi}{8}a \tag{90}$$

the value S(0), the low frequency sensitivity is given by:

$$S(0) = \frac{\upsilon P a}{8Dkl_y} \tag{91}$$

If, however, the behaviour of the function for large f, is compared to that of a first order low pass function, $H(f) = H(0)/\sqrt{1+(f/f_d)^2}$ with corner frequency f_d, then an apparent corner frequency of function ((88) could be calculated. For this apparent first order corner frequency is then found $f_d = \frac{1}{aH(0)}$, with

$$H(0) = \lim_{f\to 0} Re\left(\frac{1}{f}\left(\frac{1}{a}-\sqrt{if\frac{2\pi}{D}}K_1\left(a\sqrt{if\frac{2\pi}{D}}\right)\right)\right) = \frac{\pi a}{8}\frac{2\pi}{D} \tag{92}$$

So the diffusion corner frequency f_d (the corner frequency of the first order low pass function that has resemblance with the exact solution) is $8/\pi$ higher than the thermal diffusion frequency f_D.

$$f_d = \frac{8}{\pi} f_D = \frac{4D}{\pi^2 a^2}\,. \tag{93}$$

For the present geometries and parameters, this apparent corner frequency is higher than the thermal frequency, see Fig. 7, in which the expression for T=600K, $\Delta T(f)$ for $a=300\mu m$ and $D=7.7\cdot 10^{-5} m^2 s^{-1}$ is compared to a first order transition; the thermal diffusion frequency is $f_D = \frac{D}{2\pi a^2} = 136Hz$, whereas $f_d = \frac{8}{\pi} f_D = 350Hz$.

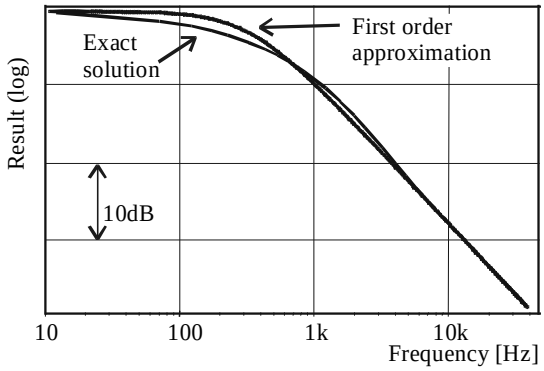

Fig. 7: Comparison of the exact solution of *ΔT(f)* and a first-order approximation.

The exact solution can be approximated by a first order function and therefore the frequency response of a Microflown can be written as:

$$|\Delta T| = \frac{vPa}{\pi D k l_y} \frac{1}{\sqrt{1 + f^2 / f_{heatcap}^2}} \frac{1}{\sqrt{1 + f^2 / f_d^2}} \tag{94}$$

This approximation consists on a product of three parts: the low frequency sensitivity, a frequency dependent (low pass behaviour) part that caused by the thermal capacity of the sensors and a frequency dependent (low pass behaviour) part that caused by thermal diffusion.

All three parts depend on the thermal diffusion coefficient, which is temperature dependent, as illustrated by Fig. 8.

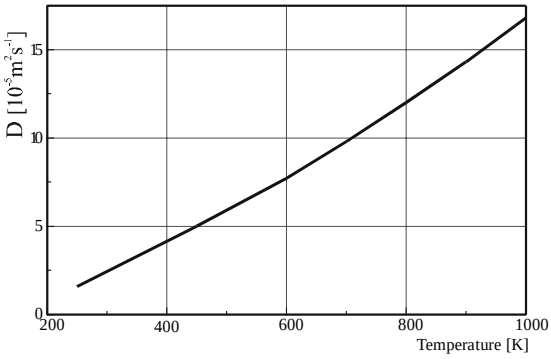

Fig. 8: Thermal diffusion coefficient as function of the temperature.

The comparison of the frequency dependence to a product of two first order low pass functions, is particularly useful when the experimental results have to be compared with theory.

Recapitulation

In the previous paragraphs models were presented that predict the temperature difference ΔT of the two sensors as result of a sound level with an (particle velocity) amplitude ν. These models are valid as long as the wires of the Microflown can be considered long and thin. Furthermore, boundary layer effects (at the position of the wires the particle velocity is zero) were neglected and the silicon nitride layer that supports the platinum sensors was not taken in to account.

A certain particle velocity is assumed width amplitude v. The transfer function between a free field (undisturbed) sound wave and the particle velocity at the position of the Microflown is not taken into account. Although it can be expected that the heaters influence the velocity profile in the sensor, and an eventual package of the Microflown would disturb the sound field as well, the measured velocity v at the heaters is assumed to be equal (or at least proportional) to the free-field particle velocity. A package such as used for the ½" ICP probe has frequency dependent phase and amplitude effects, see A2: *"package gain"*.

Acoustic phenomena consist of both sound pressure and particle velocity. For a plane wave the ratio of these two is related by the acoustic impedance, given by the product of the density and the speed of sound in the medium. Since both density and the speed of sound is temperature dependent and the temperature of the air at the Microflown is higher than its surroundings the acoustic impedance at the Microflown is lower than in open air.

The exact model of the amplitude response of the Microflown is given by Eq. (88) and the first order approximation by Eq. (94).

The phase behaviour is given by:

$$Arg\{\Delta T(f)\} = arctg\left\{\frac{f}{f_{heatcap}}\right\} + arctg\frac{Im\left\{\frac{1}{a} - \sqrt{i\frac{f}{f_D}}K_1(\sqrt{i\frac{f}{f_D}}a)\right\}}{Re\left\{\frac{1}{a} - \sqrt{i\frac{f}{f_D}}K_1(\sqrt{i\frac{f}{f_D}}a)\right\}} \quad (95)$$

The behaviour of thermal diffusion effects is described with a Bessel function K_1. The amplitude response could be accurately approximated by a first order low lass function. The phase response of the Bessel function however is clearly different from the first order response. The behaviour and difference of both are displayed in Fig. 9.

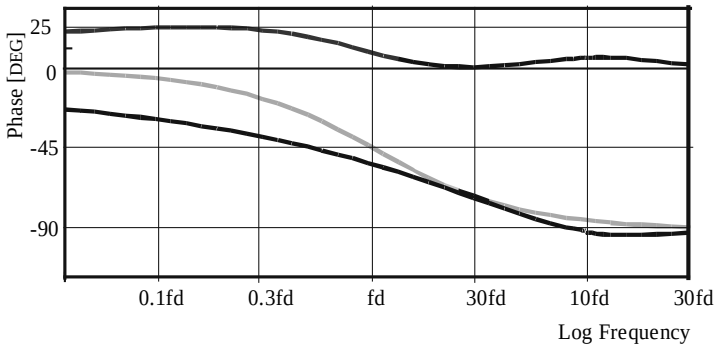

Fig. 9: Simulated phase response of a first order low pass system (grey line), of the Bessel function (lower black line) and difference of both (upper black line).

Some measurements

The low frequency sensitivity and both corner frequencies are measured as function of the spacing.

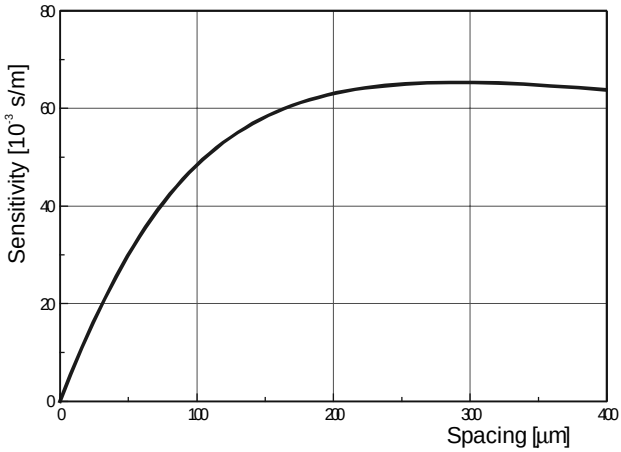

Fig. 10: Low frequency sensitivity as function of the spacing.

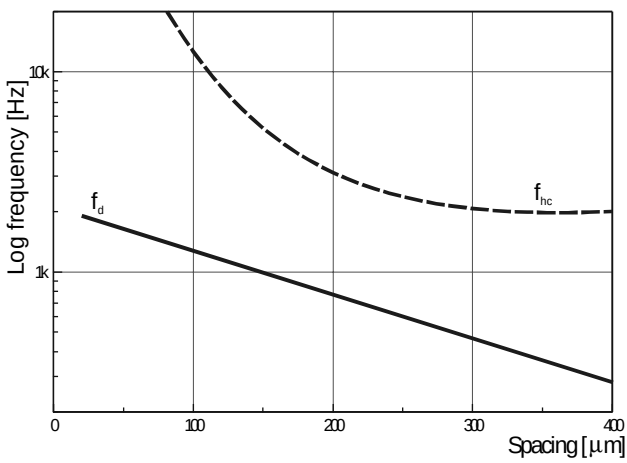

Fig. 11: Diffusion corner frequency (solid line) and heat capacity corner frequency as function of the spacing.

References

[6] V.B. Svetovoy, I.A. Winter, Model of the μflown microphone, submitted to Sensors and Actuators, Sensors & Actuators 86 (2000), 171-181.

[2] J.W. van Honschoten, G.J.M. Krijnen, V.B. Svetovoy, H-E. de Bree, M.C. Elwenspoek, Optimisation of a two wire thermal sensor for flow and sound measurement, MEMS Interlagen 2001.

Model

A2 PACKAGE GAIN

In this paragraph the effect on the frequency response of the package is examined. It shows that the sensitivity raises when a Microflown is packaged in a proper manner. It is still not completely clear what causes this so-called package gain.

There could be two effects responsible this phenomenon: The velocity is increased at the position of the Microflown due to an amplification of the particle velocity or the temperature profile of the Microflown is altered in such way that the sensitivity increases. Our feeling suggest that the first option is the major cause of the sensitivity increase. Experiments with additional package surface increase show this effect. If business cards are positioned around a ½" packaged Microflown the gain goes up an additional 10dB. Above a certain frequency the gain is dropping fast. The minimum gain is found at frequencies where the acoustic path between front and back of the Microflown is half a wavelength. Pressure gradient microphones do have similar behaviour, see chapter 2.

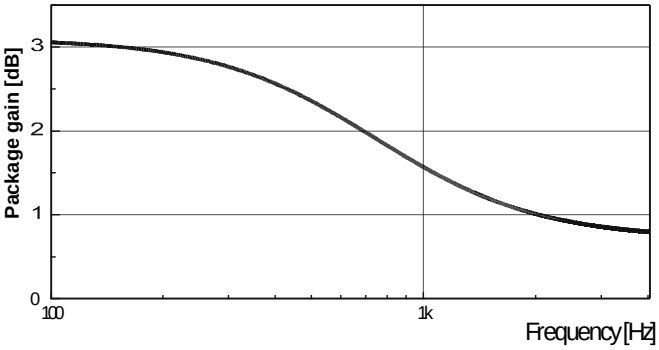

Fig. 12: Package gain due to a protecting cap over the Microflown, see Fig. 46 and Fig.77.

The gain of the ½" package is slightly frequency dependent, see Fig. 13. It is our believe that this phenomenon is caused by thermal effects. The following may be illustrate this. The effect on the sensitivity of a micromachined protecting cap is shown in Fig. 12, an example of such cap is shown in Fig. 46 and Fig.77. The cap has almost no surface so

most properly thermal effects dominate here. Another possibility is that the altered velocity distribution plays a role.

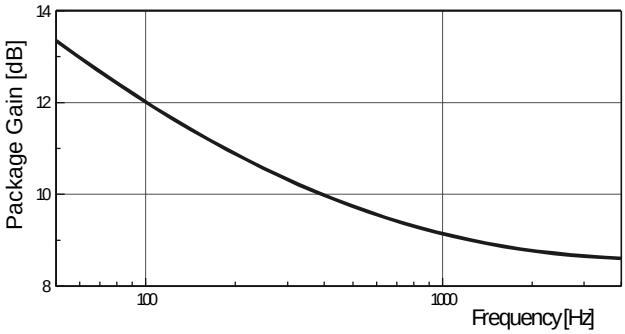

Fig. 13: Package gain of a half-inch ICP probe, see Fig. 2.18: “An example of a package with a gain of +13 to +9dB: the half inch particle velocity probe”.

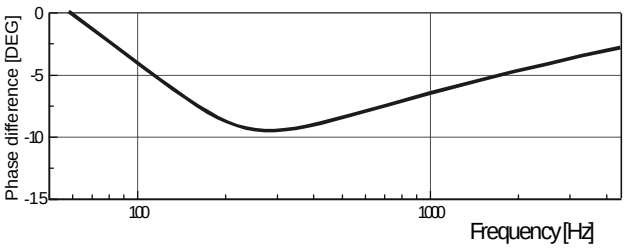

Fig. 14: The half-inch ICP probe packaging introduces a phase lag.

If the surface of the package increases, the gain goes up. This is demonstrated by the following. An additional structure is placed over the ½” package and the gain goes up again. As an example a structure of three business cards was placed around a ½” ICP Microflown. In this way a (paper) plane of 5cm×8.5cm is created with the Microflown in the middle, see Fig. 15.

The additional package gain is shown in Fig. 16. Up to 3kHz the package gain goes an additional 10dB up. At 3kHz the wavelength is 0.11m, exactly the width of the package.

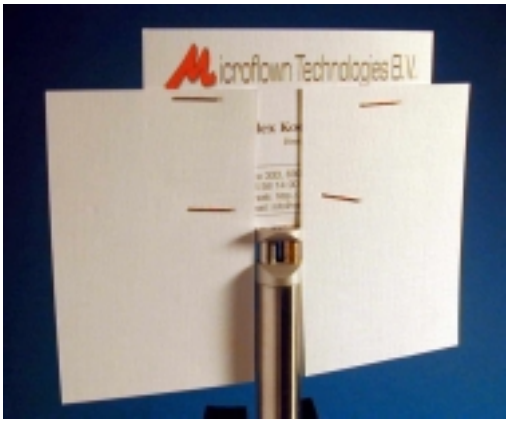

Fig. 15: Business cards cause an extra package gain.

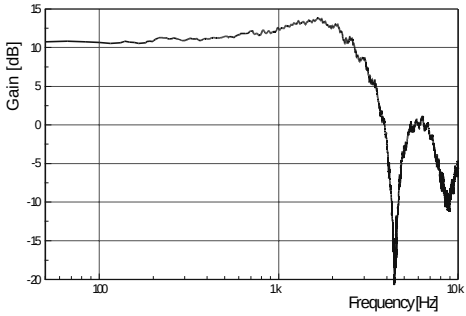

Fig. 16: Additional package gain due to business cards.

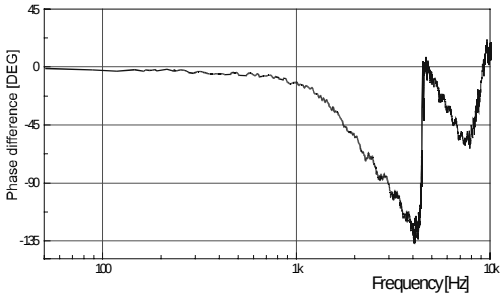

Fig. 17: Package gain due to business cards introduces an additional phase lag.

Package gain

As a last example of a high gain package, the gain of a credit card was measured. For obvious reasons we did not take my credit card, instead my medical insurance card was used.

Fig. 18: A creditcard can also cause a package gain.

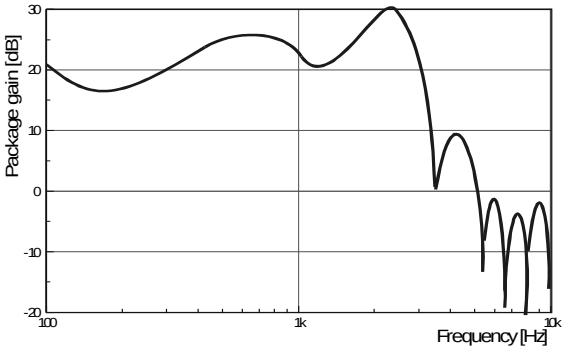

Fig. 19: A “best fit” of the measured package gain of a creditcard.

A3 THE HALF-INCH ICP MICROFLOWN, ELECTRONICS AND PERFORMANCE

The half-inch ICP probe is designed as a general-purpose particle velocity microphone. It is commercially available since 1998 and it has proven itself in many applications. It is the simplest particle velocity probe that is available.

Several connectors have become standard in the field of acoustics. The 7-pins LEMO, the BNC and the Bruel & Kjaer standard. The latter connectors are a bit bulky and outdated. We have chosen for the first two types of connectors.

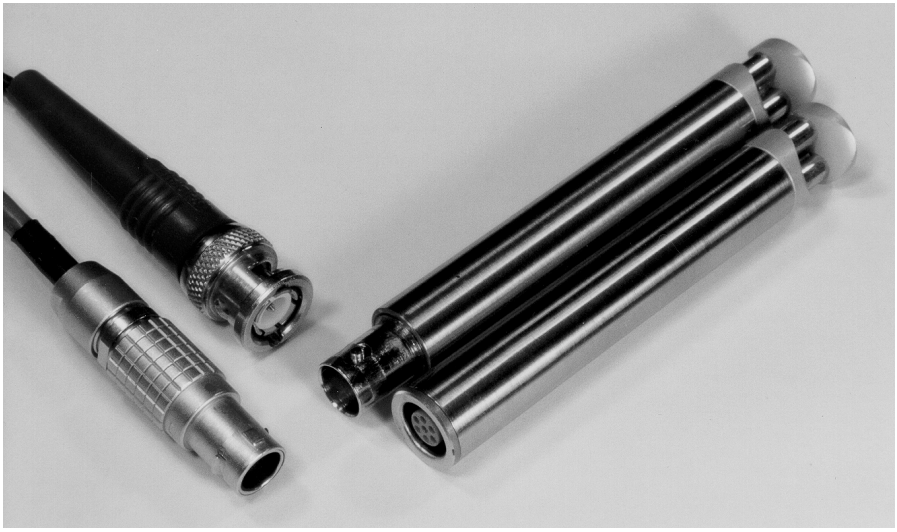

Fig. 20: ICP & LEMO Probe.

In the field of professional audio the Phantom powering (XLR connector) has become standard. A realisation of a Microflown that uses this standard is presented in chapter D2 *"Add on Microflown for a high-end pressure gradient microphone"*.

The BNC connector is a signal and shield connector only. This has as advantage that it is a very simple and low cost connector. We make use of

the unofficial) standard ICP© protocol[3]: a DC 4mA power source is powering the preamplifier and the AC voltage is used as output.

Another type of Microflown that is available (but that will not be discussed here) is the LEMO probe which connector has the advantage that it has 7-pins. Now the powering and the output can be on separate pins, which enables us to use different preamplifiers (the CE gadget, see chapter 4). The power dissipation in the probe is not limited and more functions can be implemented, like an additional miniature sound pressure microphone. Possible disadvantage is that the LEMO connector is relative expensive. A standard a 7-pins female connector is used to make it possible to use the same cables and connectors to connect a Microflown to a microphone powering-module. The LEMO realisation is discussed in chapter B: “the sound intensity application”.

The ½” ICP Microflown

The ICP preamplifier is driven by a 4mA DC current source. The ½” ICP Microflown has a single preamplifier that converts the differential resistance output of the Microflown in a varying output resistance. Due the constant current, the varying output resistor is converted in a varying output voltage. Since the ICP probe has a two-wire output it is not possible to include a correction network or a sound pressure microphone.

The ½” ICP electronics

The preamplifier of the ICP probe is given in Fig. 21. The two boxes in the middle represent a simulation of the Microflown. The resistor values are 1kΩ and varied 1‰ differential.

[3] The constant current of 4mA is a standard ICP value. The maximum voltage is 28 Volt. ICP is a registered trademark of PCB Piezotronics, Inc. (B&K has a similar system under the name CCLD (Constant Current Line Drive and HP uses the ICP standard too on its analysers).

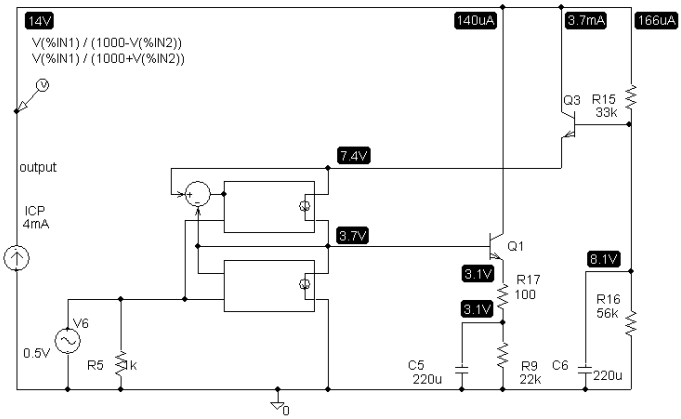

Fig. 21: PSPICE circuit of an ICP preamplifier.

The circuit is driven with a 4mA DC current source. This current is divided in three branches, the first branch (that takes 140µA) is the actual preamplifier. The second branch (3.7mA) is powering the Microflown and the third branch is converting the constant current into a constant voltage.

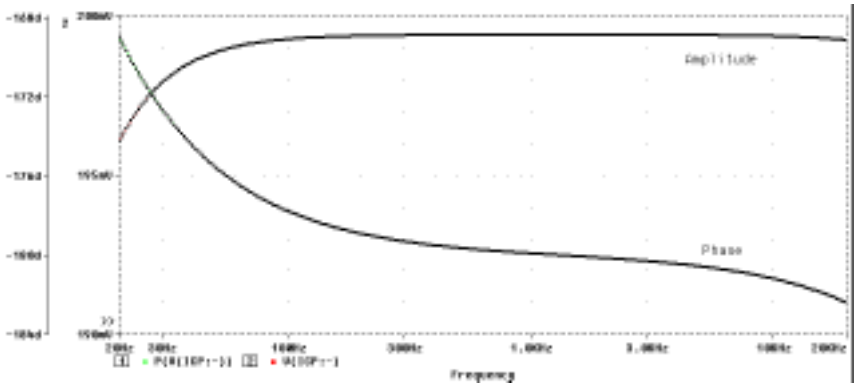

Fig. 22: The amplitude and phase response of the ICP preamplifier.

In Fig. 22 the output due to a 1‰ differential resistance variation at the input is presented. The corner frequency of the electronics that separate the AC and DC signals is around the 10Hz. As can be expected the phase response is not flat (at –180°) anymore at 10Hz. If this is

required the corner frequency has to be lowered and therefore capacitor values of C1 and C2 should be increased a factor 10 (see Fig. 21). The amplitude response is about 200mV per 1‰ differential resistance and 35mV per 1‰ common resistance variation.

The properties of the Microflown that is used are presented in chapter 4. Due to the 3.7mA current and the 7.4V voltage drop, a power of 27mW is dissipated. At this power dissipation a differential resistance variation of a 50‰ can be expected at 1m/s when a non-packaged Microflown is applied. To get a sensitivity expression that is comparable with a sound pressure microphone, this should be calculated to 2.5mm/s (94dB PVL). The differential resistor variation at 94dB is 50‰/400=0.125‰. The package gain of the ICP probe has a gain of about 12dB (4x) so the differential resistor variation of a packaged Microflown at 94dB will be 0.5‰. At this level the ICP preamplifier output should be 200mV.

A DC voltage supply and a series resistance can also operate the ICP probe. The two wires system can still be used, the resistance R_{series} converts the DC voltage in to a DC current.

½” ICP probe measurements

Frequency response / noise spectrum

The frequency response composed from three measurements, two standing wave tubes and a small anechoic chamber. The result is shown in Fig. 23. The frequency behaviour has a low frequency roll-off at 10Hz due to the ICP preamplifier electronics. The output of a ½” ICP probe due to 94dB PVL can be described like:

$$Output = \frac{245mV}{\sqrt{\left(1+\left(\frac{10}{f}\right)^2\right)\left(1+\left(\frac{f}{800}\right)^2\right)\left(1+\left(\frac{f}{1300}\right)^2\right)}}$$

The noise is measured in a 1Hz bandwidth so the noise spectrum that is presented in Fig. 23 is given in dB(V)/√Hz.

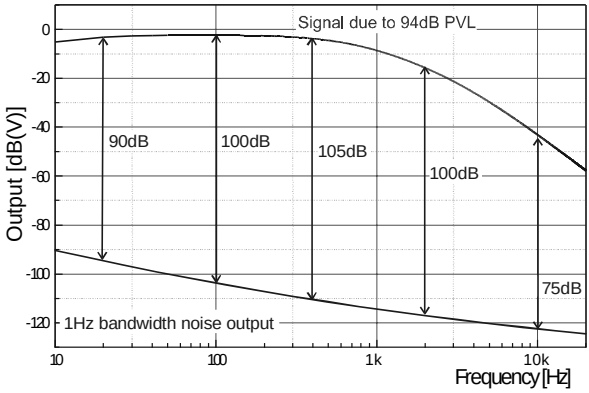

Fig. 23: Output of a ½" ICP Probe: the signal is due to 94dB PVL, the noise spectrum is given in dB(V)/√Hz.

Phase response

The phase response of a half inch ICP Microflown are depicted in Fig. 24. The measured phase response can be fitted by:

$$Phase = -1.68 \cdot tg^{-1}\left(\frac{f}{950}\right) \tag{96}$$

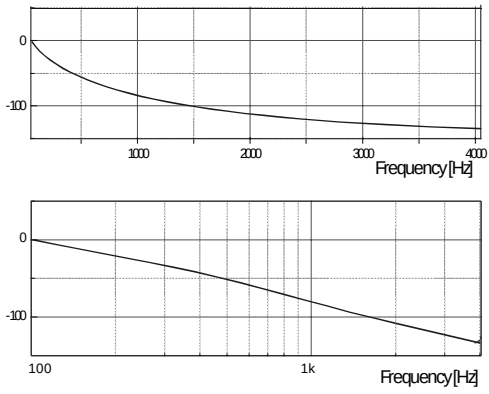

Fig. 24: Phase response of a half-inch ICP probe.

Linearity

The linearity of a half-inch ICP probe is reduced for higher sound levels due the electronics. In a measurement the level is raised until the second harmonic becomes –30dB relative to the first harmonic. Results are shown below,

Frequency	Sound level
150Hz	100dB
775Hz	100dB
2370Hz	120dB
3950Hz	100dB

Polar pattern

The polar patter was measured in a standing wave tube. The results are depicted in Fig. 25. Values are presented in a linear way so that the cosine shape becomes clear.

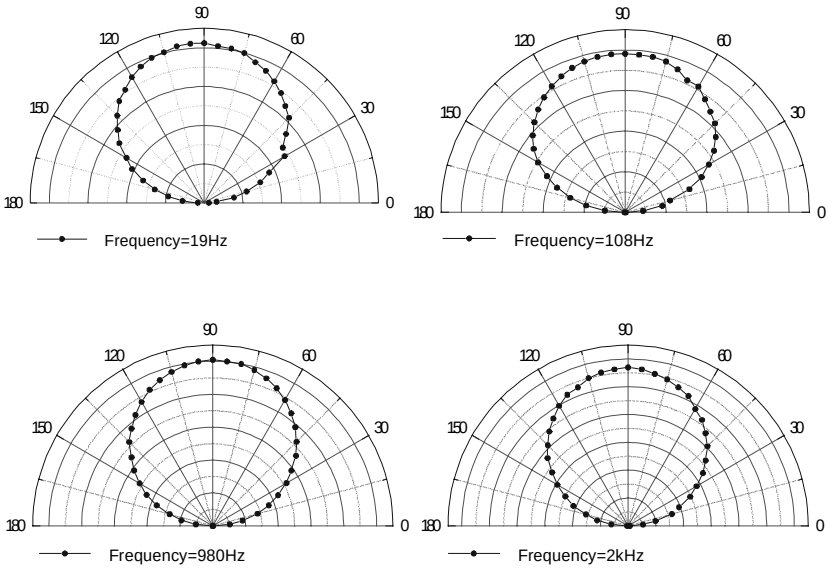

Fig. 25: Polar patterns of a ½” ICP Microflown at different frequencies.

The ratio between on- and off-axis are also measured for several frequencies. The measurements took place in a standing wave tube so it is possible that some off-axis noise was present. The values that are given could be better under anechoic conditions.

Ratio between on- and off-axis are also measured for several frequencies			
30Hz	30dB	1400Hz	60dB
71Hz	65dB	2kHz	66dB
117Hz	50dB	3kHz	45dB
250Hz	45dB	4kHz	25dB
800Hz	49dB		

A4 STATISTICAL DATA ON THE ACOUSTIC PERFORMANCE OF MICROFLOWNS

Fourteen non-packaged Microflowns where measured in a calibration standing wave tube, see chapter AV: *"calibration methods"*. The voltage over the Microflowns was 8V, the average low frequency output was -26.75dB reference to a sound pressure microphone with a sensitivity of 14mV per Pascal. So the low frequency sensitivity of the Microflowns is 0.64mV/Pa* = 257mV/m/s. The supply voltage was 8V so the differential relative resistance variation can be calculated: 0.16‰ per Pa* which equals 64‰ per m/s.

The diffusion corner frequency of the average response of is modelled 450Hz and the heat capacity corner frequency 1350Hz.

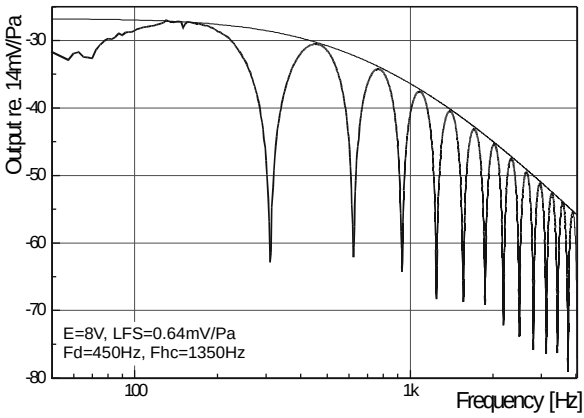

Fig. 26: Average frequency response of fourteen non-packaged Microflowns in a standing wave tube relative to a pressure microphone at the end of the tube with a sensitivity of 14mV/Pa (thin line represents the model).

The standard deviation of the frequency response of the fourteen Microflowns is given in Fig. 27. The minimal deviation is about 0.27dB. The impedance tube causes the higher deviation at frequencies below 100Hz: the tube should not be used below 100Hz. The enlarged deviation peaks are caused by the calibration method rather than by the Microflown itself.

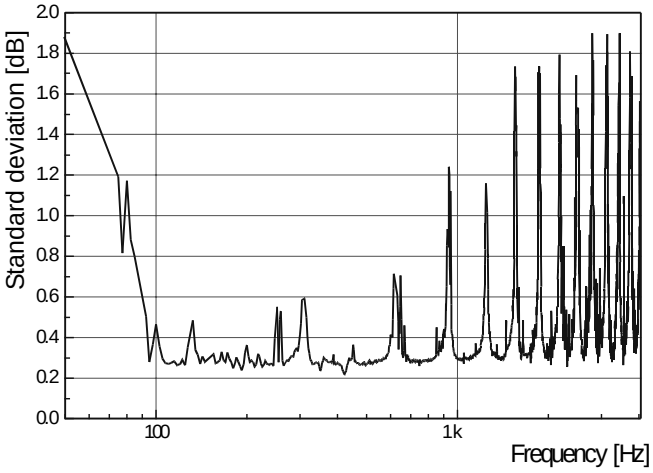

Fig. 27: The standard deviation of the frequency response of fourteen non-packaged Microflowns in a standing wave tube.

The average phase response of the fourteen non-packaged Microflowns is depicted in Fig. 28. As can be seen, when the tube is in resonance the phase response of the Microflown in the standing wave tube deviates strongly. This is an effect of the tube rather than the Microflown. See also paragraph A5: "*calibration methods*". The standard deviation of the phase response of the fourteen Microflowns in a standing wave tube is depicted in Fig. 29. Apart from the tube's resonance the deviation for lower frequencies is about 0.5 degrees. At higher frequencies this figure is increasing. It is likely that the calibration method (at higher frequencies the calibration of the phase becomes more difficult) causes this deviation increase.

Here the phase and amplitude response is measured at one position in the tube. The distance between the reference microphone and the Microflown is taken large. Better calibration results can be expected when this distance is taken small.

Similarity

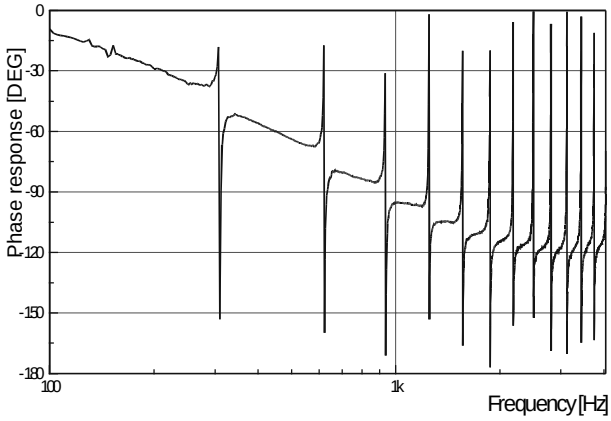

Fig. 28: Phase response of ten naked Microflowns in a standing wave tube.

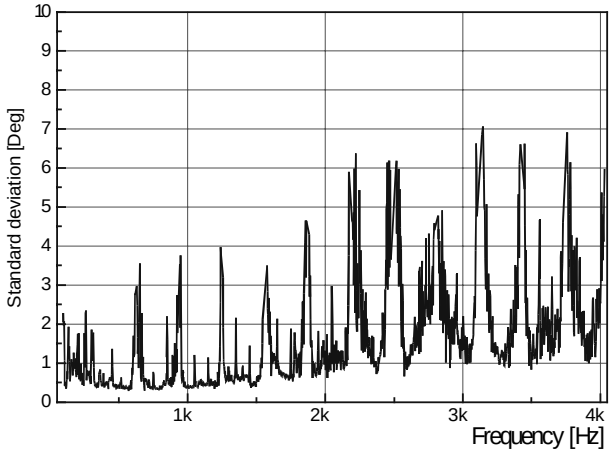

Fig. 29: The standard deviation of the phase response of fourteen non-packaged Microflowns in a standing wave tube.

Similarity

A5 CALIBRATION METHODS

Several calibration methods to determine the frequency response of the Microflown have been tested over the years. Three methods came out best: an anechoic calibration, a standing wave tube calibration and a time frame method in a long tube. Pros and cons as well as theory and examples of measurements will be discussed here. This chapter is based on the work that is presented in [1-5].

Some alternative methods of calibration can be found at chapter B2: "*a p**u** sound intensity measurement*"

Introduction

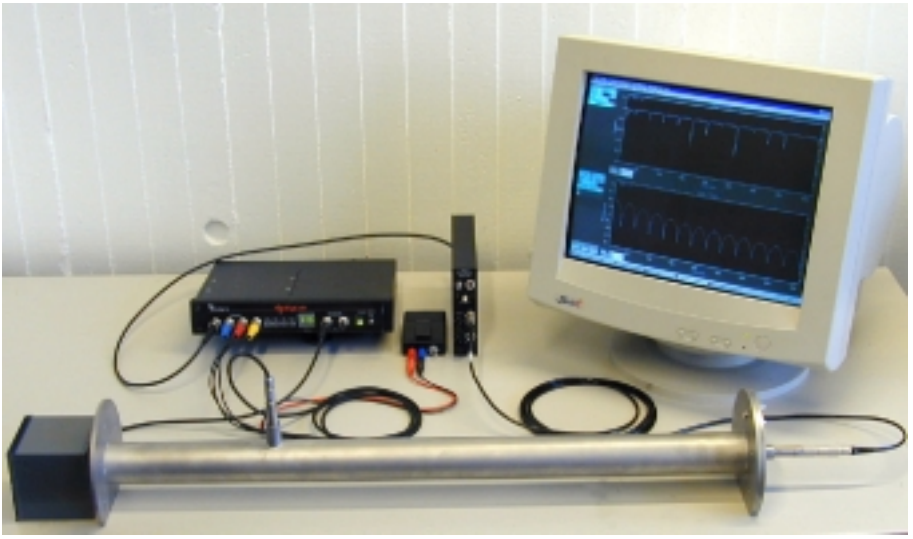

Fig. 30: Standing wave measurement set up is used to calibrate the Microflown in a frequency range from 100Hz to 4kHz.

Since a reference particle velocity microphone doesn't exist, the main concern calibrating the Microflown is to offer a known particle velocity to the probe. Measuring the sound pressure in a configuration in where the specific acoustic impedance is known solves this problem. The

particle velocity is calculated by dividing the sound pressure with the specific acoustic impedance, see chapter 2.

Three methods to measure the transfer function of the Microflown will be presented. Pre and cons will be discussed on useful bandwidth, ease of use and expense.

The anechoic room, an environment with a simple sound source and non-reflecting walls, will approach free field conditions. The method is easy to use and most reliable but it is a very expensive set-up. It can be used in a 50-20kHz bandwidth.

A low cost solution to approach free-field measuring conditions is to measure in a long tube by means of time frame measurements. The practical effective bandwidth is limited by diameter and length of the tube and is found several kilohertz. The particle velocity and the sound pressure in these two set-ups are simply related.

The situation in a standing wave tube is a bit more complex but the set-up is small and low cost. With some effort, the underlying mathematics can be understood quite easily. By the use of two standing wave tubes, a bandwidth of 10Hz up to 4kHz can be achieved.

The anechoic chamber

A room with sound-absorbing or reflection-free walls is called an anechoic chamber. Since in such environment no reflections are present a *free field* measurement can be performed: all the sound is coming from one place in space. The specific acoustic impedance must be known to calibrate the Microflown. The sound pressure on one position can be measured quite accurate with a microphone and the particle velocity can be calculated by dividing the sound pressure by the specific acoustic impedance. For a free spherical sound wave the impedance is given by (see also chapter 2):

$$z(r) = \frac{p(r,t)}{u_r(r,t)} = \rho_0 c_0 \left(\frac{ikr}{ikr+1} \right) \tag{97}$$

The wave number k equals ω/c (ω=2πf using f as the frequency). If the product kr is much larger than unity the relation will alter in:

$$z(r) = \rho_0 c_0 \tag{98}$$

So, if the microphones are located “far” from the source the specific acoustic impedance is a real and constant figure and this, of course, makes the calibration relatively simply.

The most uncomplicated way to be able to perform anechoic measurements is in an open field: a loudspeaker is put on the ground and above it the sound field can be considered as a “free field”. This works rather well (see chapter 1 and B2) but is, due to weather conditions, not always convenient

Anechoic chambers cannot be used at lower frequencies since it is very difficult to absorb low frequency sound waves. Anechoic chambers that can be used down to 50Hz have sound absorbers that are one to two meters thick. Such chambers are therefore large, $10\times10\times10\text{m}^3$ can easily be expected.

An anechoic chamber that can be used for frequencies higher than 1kHz can be made much smaller. The sound absorbing layer can be made of 10cm absorbing foam and outer dimensions can be as small as $1\times0.7\times0.7\text{m}^3$. To get the acoustic impedance to be a real figure, the sound probe should be relative far from the sound source. For frequencies higher than 1kHz, 30cm distance from the source can be considered far: $kr = 2\pi\times1000/330\times0.3 = 5.7>>1$. Measurement results in the small anechoic chamber are shown in Fig. 40.

Some (inferior) anechoic rooms use a so-called pressure correction. By a feedback loop the sound volume of the loudspeaker is adjusted in such way that the sound pressure at the reference microphone is constant for all frequencies. The result of possible reflections will be eliminated for pressure transducers. This trick works rather well if a sound pressure microphone has to be calibrated but it will produce large errors if a velocity (or pressure gradient microphone) is under investigation. Observe the ripples in the anechoic measurement result that is depicted in chapter 1, Fig. 1.11.

Compared to measurements in a tube, the sound levels are normally quite low (50dB-70dB) in an anechoic room. This is because the sound wave can propagate in all directions and therefore its power will decrease with the square of the distance. In a tube the sound wave is “trapped” and sound powers can easily reach 120dB.

The long tube

For measuring frequencies in the range from 50Hz to 2.5kHz a long tube is used (ordinary PVC rain-pipe). The idea behind this set-up is that the acoustical impedance of a tube with no reflections at the end has a characteristic impedance ($Z_s=\rho c$), same impedance as a free field measurement).

When a sine burst is applied, a measurement can take place before a reflection returns. At least ten periods have to be measured to ensure consistency. This implies that the lowest possible frequency to measure is given by the following formula:

$$f_{\min} = \frac{10 \cdot c}{2 \cdot l} \approx \frac{1700}{l} \tag{99}$$

Using l as the distance from the Microflown and microphone and the end of the tube. So for a forty-meter long tube the lowest frequency which could be measured should be about 50Hz. The spacing between the loudspeaker and the microphones is used to be sure that the acoustic waves are plane; non-plane waves will vanish exponentially. It will also introduce a time delay that which ensures that the output signal of the Microflown is not an electro-dynamic transduction, because in this case the time delay will be much shorter.

Above the cut-off frequency the specific acoustic impedance changes due to the existence of standing waves perpendicular to the direction of the sound wave. The set-up will then be very difficult to use since the acoustic impedance is not a real figure anymore. For a tube this cut-off frequency is given by:

$$f_c = \frac{c}{1.71 \cdot d} \tag{100}$$

Where d represents the diameter of the tube, and c the speed of sound (approximately 330m/s). It is rather difficult to measure high sound intensity levels below the 100Hz in the seven centimetre tube while the loudspeaker becomes very non linear as it has the same (small) diameter as the tube. Measurements will generally be reliable if sound levels below sixty deci-Bell are used.

Calibration methods

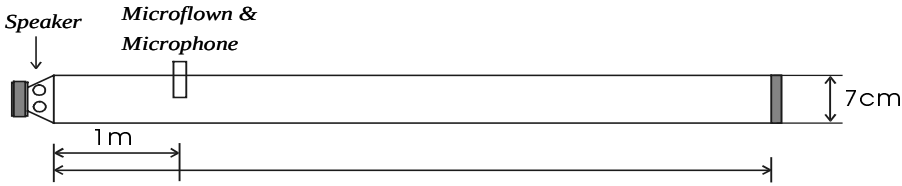

Fig. 31: The 40m long tube measurement set up is used to calibrate the Microflown in a frequency range from 100Hz to 2.5kHz.

The measurements are performed using acoustic bursts. A typical measurement is shown in Fig. 32. One burst provides one (phase and amplitude) point in the transfer function. Normally four hundred measurements are made in the frequency range from one 50Hz to 2.5kHz. It takes about 30 seconds for the sound wave is vanished. So it takes 30 seconds to measure one point in the frequency spectrum.

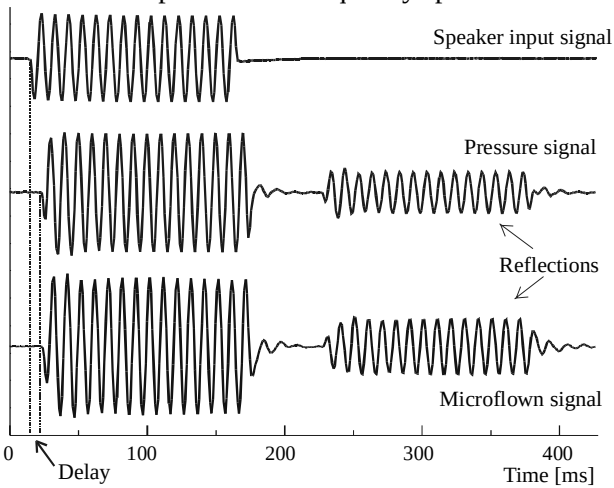

Fig. 32: A typical measurement in the ‘infinite’ tube providing one point of the transfer function.

The difference in response of a microphone and a Microflown can be seen in Fig. 32; the sound pressure signal and the Microflown output are in phase the first time the acoustic burst passes and they are out-of-phase at the after the first reflection.

Standing wave tube (SWT)

In a tube the acoustic waves are plane below the cut-off frequency, see Eq. (100). The sound wave can only travel in one direction. In a standing wave tube, a rigidly terminated tube with rigged sidewalls, the all sound will be reflected at the end of the tube.

The specific acoustic impedance inside the SWT can be calculated by solving the wave equation. The fluid is excited by a piston (or a loudspeaker) with amplitude U at the left-hand end and is terminated by a rigid boundary at the right hand end, see Fig. 33.

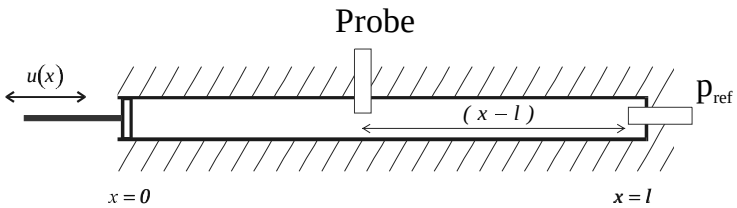

Fig. 33: A tube that is rigidly terminated at x=l and in which the fluid is driven by a vibrating piston at x=0.

For harmonic excitation, one solution that will satisfy the wave equation is given by the superposition of the complex pressures associated with a positive travelling and a negative travelling plane wave. The plane wave approximation is allowed for frequencies lower than the cut off frequency, see Eq. (100). In general the pressure is given by:

$$p(x) = Ae^{-ikx} + Be^{ikx} \tag{101}$$

Where A and B are arbitrary complex numbers ($i^2=-1$) which represent the amplitude and relative phases of waves travelling in the positive and negative x direction respectively, k is known as the wave number and equals $k=\omega/c$ ($\omega=2\pi f$ using f as the frequency).

The particle velocity associated with this pressure wave can be found using the linearised momentum equation ($\partial p(x)/\partial x=-i\omega\rho u(x)$).

$$u(x) = \frac{Ae^{-ikx}}{\rho c} - \frac{Be^{ikx}}{\rho c} \tag{102}$$

The values of the complex constants A and B are solved knowing that the particle velocity is zero at $x=l$: $Ae^{-ikl} = Be^{ikl}$ and at the left hand side of the tube the particle velocity is given by the movement of the piston $u(0)=U$: $\rho cU = A - B$. The sound pressure and particle velocity at any place in the tube are given by:

$$p(x) = -i\rho cU \frac{\cos(k(l-x))}{\sin(kl)} \qquad u(x) = U \frac{\sin(k(l-x))}{\sin(kl)} \tag{103}$$

The specific acoustic impedance at place x in the tube is given by:

$$Z_s = \frac{p(x)}{u(x)} = -i \cdot \rho c \cdot \cot(k(l-x)) \tag{104}$$

As can be seen the specific acoustic impedance in a closed tube does not equal the characteristic impedance but it is a co-tangent function that varies from plus to minus infinity. Such function is not very suitable to use for the calibration, see Fig. 33. A good place to put a reference microphone is at the end of the tube since the sound pressure is at its maximum at that place; so $p_{ref}.(x=l)=p_{ref}.(l)\equiv p_{ref}$.

If a p-**u** sound intensity probe is put at a certain position x in the tube the relation between the pressure microphone of the p-**u** sound intensity probe and the reference (pressure) microphone at the end of the tube is given by: ($p_{probe}=p_{probe}(x)$).

$$\frac{p_{probe}}{p_{ref.}} = \cos(k(l-x)) \tag{105}$$

The relation turns out to be a simple cosine function. The distance (l-x) can easily be obtained by measuring two minima of the cosine function.

Analogously, almost the same applies for the particle velocity ($u_{probe}=u(x)$):

$$\frac{u_{probe}}{p_{ref.}} = \frac{i}{\rho c}\sin(k(l-x)) \tag{106}$$

The relation of the particle velocity and the reference sound pressure at the end of the tube turns out to be a simple sine function. The phase shift between them equals plus or minus 90 degrees.

It shows that for calibrating the p-**u** probe for obtaining the sound intensity only the phase mismatch (φ_p-φ_u) should be determined and individual phase mismatch of both probes does not have to be determined. The p-**u** probe phase mismatch (φ_p-φ_u) can be determined by measuring the ratio of the particle velocity and the sound pressure in the tube. The equation of the ratio is given by:

$$\frac{u_{probe}}{p_{probe}} = \frac{i}{\rho c} tg(k(l-x)) \rightarrow Arg\left\{\frac{u(x)}{p(x)}\right\} = \pm 90^{\circ} \tag{107}$$

This relation shows that in a standing wave tube particle velocity and sound pressure are 90 degrees out of phase. In this way the p-**u** probe is phase calibrated in the arrangement as it is used: the pressure microphone is positioned face to face to the Microflown.

An accurate model of the standing wave tube measurement

The models that are presented in the previous paragraph are valid under ideal situations. In practice however the sound in the tube is slightly damped. Two effects cause this. The particle velocity is zero at boundaries of the tube. In the middle of the tube the sound wave propagate as a plane wave. The friction in the air between zero velocity and plane wave causes damping. This effect is noticed most at low frequencies. At high frequencies the damping of the air itself will be noticeable. If the standing wave tube is dimensioned in a proper manner, the effects will be hardly noticeable.

If thermal viscous effects (damping) are taken into account, Eq. (106) will alter in to [1], [2]:

$$\frac{u_{probe}}{p_{ref.}} = \frac{i}{\rho c} \frac{sinh\,\Gamma(k(x-l))}{\Gamma} \tag{108}$$

Using Γ as the viscothermal wave propagation coefficient which is given by:

$$\Gamma = i + \frac{1+i}{\sqrt{2}}\left(\frac{\gamma - 1 + \sigma}{s\sigma}\right) \tag{109}$$

Using γ=1.4 ratio of specific heats of air, σ=0.845 square root of the Prandtl number and *s* as the shear wave number:

$$s = \frac{d\sqrt{\omega}}{2}\sqrt{\frac{\rho}{\mu}} = 346\,d\sqrt{f} \tag{110}$$

Using $\mu=17.1\cdot10^{-6}$ [Pa s] as the dynamic viscosity and $\rho=1.3$ [kg/m^3] as the density. To use this model the shear wave number must be much larger than unity, which is in practical cases true. For several shear wave numbers the particle velocity amplitude profile is depicted in Fig. 34. The viscothermal wave propagation coefficient can be simplified to:

$$\Gamma = i + \frac{1+i}{332d\sqrt{f}} \tag{111}$$

As can be seen, for higher frequencies or large diameters, Γ will reach i. If $\Gamma=i$ is substituted in Eq. (108), it will alter into relation Eq. (106).

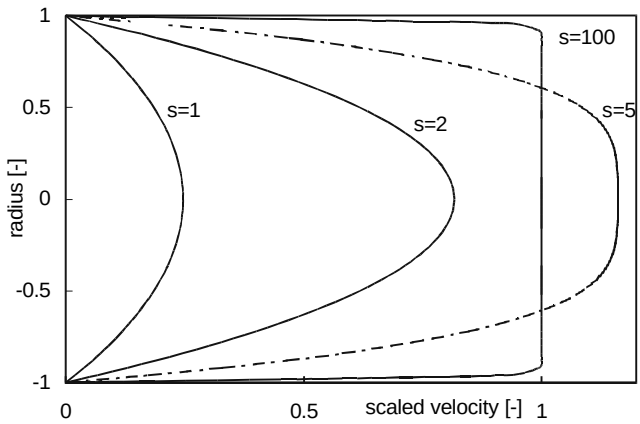

Fig. 34: Particle velocity profile as function of the shear wave number.

One should dimension the diameter and the length of the tube in such way that the factor 332d√f is as large as possible. For low frequencies we use a tube of 16cm in diameter and 8meters in length. In this case, at 20Hz the effect of damping is not noticeable. The tube can be used up to 1kHz due to the corner frequency of the tube, see Eq. (100). For higher frequencies we use a tube that is 4.5cm in diameter and 1meter in length.

This tube is used in a 50Hz-4kHz bandwidth. For half-inch probes, it is not possible to use smaller tubes.

Although the thermal viscous effects are relative small, they are observed most clearly in the phase response. The phase response in the tube should be plus or minus 90 degrees (see Eq. (106)) however the measured response shows "rounded edges", see Fig. 37. This is due to these thermal viscous effects.

A standing wave tube measurement

To get a “feeling” of measured signals in the tube, some signals were measured in a standing wave tube of l=98cm in length and 9cm in diameter, the position of the pressure a microphone and the Microflown is *(x-l)*=47cm. The reference microphone is placed at the end of the tube. The tube can be used up to 2kHz, see Eq. (100).

To avoid a mechanical transfer function between the loudspeaker and the sound probes, the loudspeaker should not be mounted rigidly to the tube.

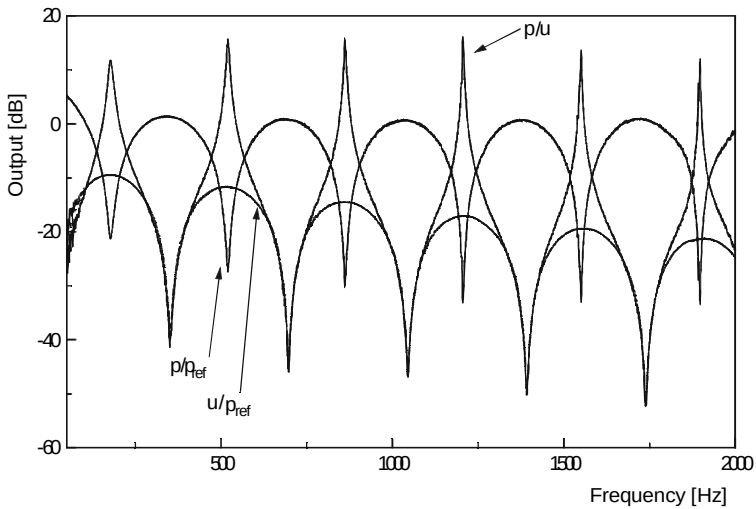

Fig. 35: Measurement in a standing wave tube: the sound pressure p, particle velocity u and the specific acoustic impedance (the ratio of both p/u).

The measurements in the standing wave tube are performed with a dual channel analyser and as reference microphone at the end of the tube

a half-inch pressure microphone is used (type GRAS 26AC). In Fig. 35 the frequency response of a microphone and Microflown (at position *(x-l)*=48cm)) divided by the output of the reference microphone at the end of the tube, see Eq. (2.10) and Eq. (106) is depicted.

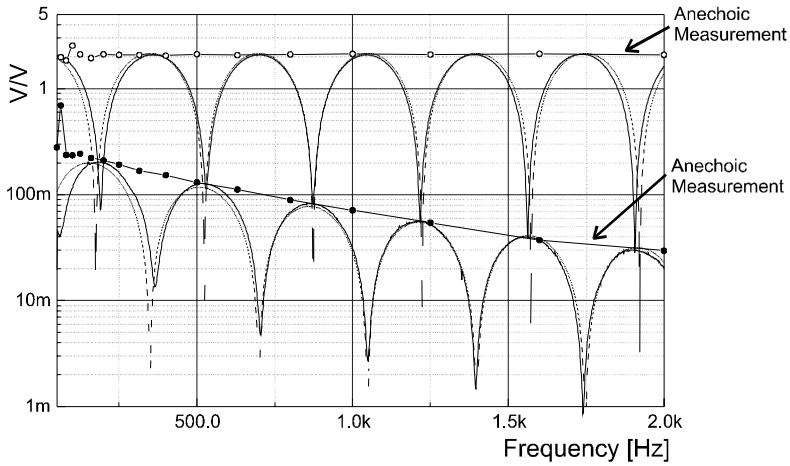

Fig. 36: Measurement and simulation results. The upper curves represent the calibration of the pressure probe and the lower curves the calibration of the Microflown. The solid lines are measurements, the dashed lines simulation results.

According to theory a maximum for the sound pressure can be expected when a minimum for the particle velocity is found; and vice versa. As can be seen, the frequency response of pressure microphone is flat. Here a Microflown is used with a corner frequency of 500Hz. For higher frequencies the sensitivity decay is clearly noticeable. The value *(l-x)* in respectively Eq. (2.10) and Eq. (106) can easily be determined from the measurement. The minima of the cosine function appear every π rad, the frequency difference between the minima is 345Hz and therefore:

$$\Delta k(l-x) = \frac{2\pi\,\Delta f}{c}(l-x) = \pi \rightarrow (l-x) = \frac{c}{2\,\Delta f} = 0.49m \qquad (112)$$

The equations Eq. (2.10) and Eq. (106) can be rewritten to predict the frequency response as depicted in Fig. 36. The frequency response of the pressure microphone is flat but the frequency response of the Microflown shows a low-pass frequency behaviour. This should also be taken into account:

$$\frac{p_{probe}}{p_{ref.}} = \left| cos(0.49\frac{2\pi}{c} f) \right| \frac{u_{probe}}{p_{ref.}} = \frac{\left| sin(0.49\frac{2\pi}{c} f) \right|}{\rho c\sqrt{\left(1+\left(f/_{700}\right)^2\right)\left(1+\left(f/_{2000}\right)^2\right)}} \quad (113)$$

In Fig. 36 the various results are displayed: the anechoic calibration of the pressure microphone and the Microflown, the standing wave tube calibration results and the simulation results of Eq. (113). As can be seen the measurements are in good agreement with the theory.

A calibration measurement

The anechoic phase curve decays from -30 degrees down to -125 degrees. Since the Microflown has a first order frequency behaviour, a corresponding phase curve from 0 down to -90 degrees should be expected. In this realisation the preamplifier of the Microflown has a phase lag of about 30 degrees; the phase mismatch of the pressure microphone (plus preamplifier) also varied a few degrees in the observed bandwidth.

According to theory the anechoic phase response should differ plus or minus 90 degrees from the standing wave phase response, see Eq. (107). The measurement results showed in Fig. 37 are in reasonable agreement with the theory.

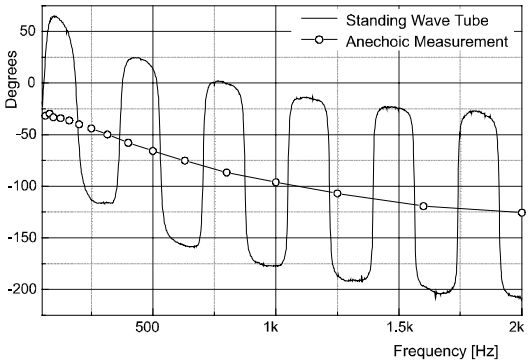

Fig. 37: Phase difference between the output of a microphone and a Microflown of a p-**u** sound intensity probe. Solid line: measured in the standing wave tube and line with circles is measured in the anechoic room. The rounded edges of the solid line are due to damping effects.

Amplitude measurements in a small standing wave tube

To show the calibration method as explained by Eq. (2.10) and Eq. (106) a sound pressure microphone and a ½' ICP Microflown are calibrated in the standing wave tube that is displayed in Fig. 30.

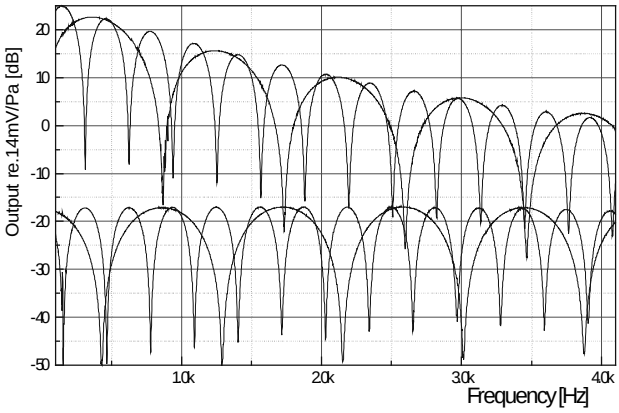

Fig. 38: Amplitude response of ½" ICP probe (upper curves) and a ½" sound pressure microphone (lower curves). The length (x-l) is varied from 20cm to 55cm (the reference microphone and the loudspeaker change in position), see Fig. 30. The accompanying phase response of a Microflown is shown in Fig. 39.

At the minima it is not possible to calibrate the Microflown. To overcome this problem the tube can be used in two ways. The reference microphone can be mounted on both sides of the tube. Furthermore, the position of the mounting of the probe is made not symmetrical. So by altering the position of the loudspeaker and the microphone, the distance *(x-l)* is varied from 20cm to 55cm, see Fig. 30. The results of reconfiguring are shown in Fig. 37. The tube that is displayed in Fig. 30 is tube is 1meters in length and 4½cm in diameter so the maximal frequency it can be used is 4200Hz. The lowest frequency of which the tube can be used is about 50Hz.

Standing wave tube (phase); probe rotation [4]

The phase shift between particle velocity and sound pressure in a standing wave tube is ±90°. The phase shift between a sound wave coming from the front or behind a Microflown equals 180°. So if two

phase-responses in a standing wave tube are measured and averaged, in theory the free field phase response is obtained, see Fig. 37. Only at the frequencies where the tube-response shifts from +90° to -90°, the average value seems to ripple. This is caused by the damping of the tube.

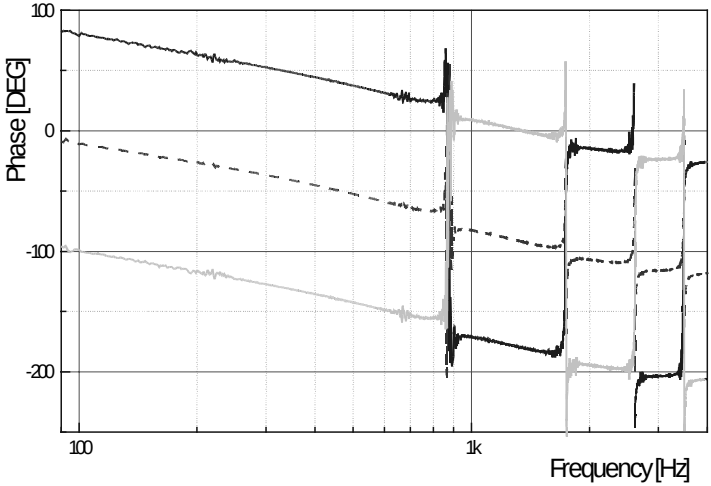

Fig. 39: Phase response of a ½" ICP probe. Solid black: in phase, solid grey out of phase, dotted average of in and out of phase. The length *(x-l)* equals 20cm, see Fig. 30.

Broadband calibration

For the broadband calibration of a ½" ICP probe three measurements set-ups are used. For low frequencies, 20Hz-1kHz, a 8 meters long standing wave tube was used with a diameter of 16cm. The material of the tube is simple PVC. In the frequency band from 100Hz up to 4kHz the small standing wave tube is used, see Fig. 30. The highest frequencies are covered in the small anechoic chamber that is treated in a previous paragraph "*the anechoic chamber*".

As can be seen in Fig. 40 the responses match quite well. The anechoic response shows some ripples. It is most likely that these are caused by reflections in the chamber. It is also noticeable that the response at lower frequencies has a slight decay. This could be due to the

damping of the tube or due to the electronic filtering of the preamplifier of the ICP probe.

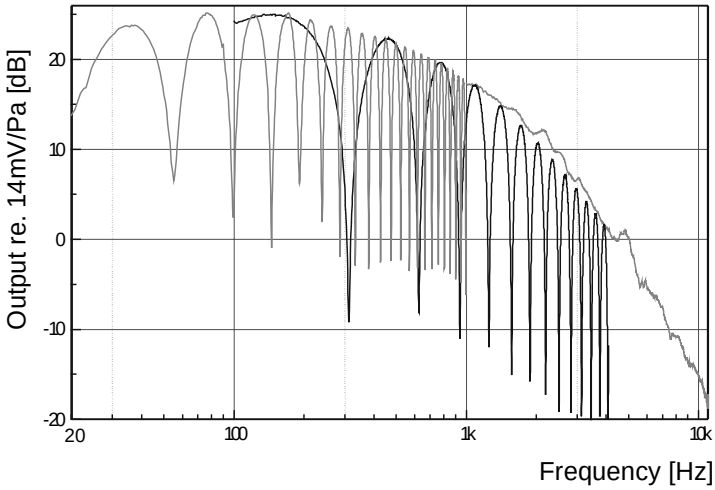

Fig. 40: Amplitude response of ½" ICP probe in a large (8m/16cm) standing wave tube (grey line, 20Hz-1kHz), in a short (75cm/4,5cm) standing wave tube (black line, 100Hz-4kHz) and in a small (1m^3) anechoic room (grey line, 1kHz12kHz).

Conclusion

Three calibration methods are presented the anechoic room, the long tube and the standing wave tube.

A large and high quality anechoic room can be used from 50Hz up to 20kHz. Such rooms are very expensive. A small (and inexpensive) chamber can be used from 1kHz up to 20kHz.

A long tube (40 meters) can be used from 50Hz up to 4kHz. The calibration of the Microflown is quite easy but it will take more time than calibrating it in the anechoic room or standing wave tube and the analyser that is needed to calibrate is also more complex: it must be capable to perform time frame measurements.

A set of standing wave tube of acceptable dimensions can be used from 15Hz up to 4kHz. An 8 meters and 15cm diameter tube has a frequency span from 15Hz up to 1kHz and a 75cm, 5cm diameter tube

has a frequency span from 100Hz up to 4kHz. The calibration is a bit more complex as calibrating in an anechoic room.

The best way to calibrate a Microflown in the full acoustic bandwidth (20Hz up to 20kHz) is a combination of a small anechoic room and two standing wave tubes. In the standing wave tubes the responses from 15Hz up to 4kHz are measured and in a small anechoic room the response for frequencies higher than 1kHz is obtained.

References

[1] H-E. de Bree, W.F. Druyvesteyn, M. Elwenspoek, Realisation and calibration of a novel half-inch p-u sound intensity probe, 106th AES Munchen, 1999.

[2 J.W.van Honschoten et al, The influence of viscothermal effects on calibration measurements in a tube, presented at the LA AES 2000.

[3] H-E. de Bree et al, A novel technique for measuring the reflection coefficient of sound absorbing materials, ISMA25, International Conference on Noise and Vibration, September 13-15, 2000 - Leuven, Belgium.

[4] Private discussion with R. Raangs.

[5] H-E de Bree, The Microflown, Ph.D. thesis, H-E de Bree, ISBN 9036509262, 7 February 1997.

A6 A COMPARISON BETWEEN A SOUND PRESSURE MICROPHONE AND A MICROFLOWN

The characteristics of the Microflown and a condenser microphone are compared based on acoustical, electrical and other properties. The acoustical properties that are considered are selfnoise, bandwidth, upper sound limit and sensitivity. The electrical properties are operating power and supply voltage. The other properties on which both microphones are compared are matters like size and environmental durability.

Introduction

It is very difficult to compare one microphone with another without mentioning the purpose of using the device. Microphones can be found in many prices, qualities and shapes. For comparison the average values five of types of pressure microphones will be examined:

- a low cost electret microphone (0.25€)
- a 0.1” miniature microphone (15€)
- a high end studio microphone (1500€)
- a high end pressure gradient studio microphone (1500€)
- a half inch microphone for measurement purposes (2000€)

The numbers behind the types indicate the market price of these microphones (1€≈1USD).

The low cost microphone is used in mass productions such as toys. These microphones do have a quite good acoustic quality. The stability however is very poor. The miniature microphone is used in hearing aid equipment. Despite the smaller dimensions, the acoustic quality is similar to the low cost microphone. The studio microphones have got a much better acoustic quality than the low cost microphone. This shows particularly due to a high linearity and low selfnoise. High stability, very high linearity and a high bandwidth are the main properties for a measurement microphone. Often precautionary measures are taken to

avoid moisture problems. The selfnoise in mostly not as low as a studio microphone.

The Microflown could very well be used as a low cost microphone. The noise figures are within reasonable (30dB(A)) limits and the price should competitive if it is mass-produced. One possible disadvantage can be it higher power consumption (10mW).

The Microflown will perform also well as a miniature microphone. Especially when the power consumption and noise figures is of less importance (measurement purposes). The technology is not yet suited for hearing aid applications. Hopefully a new generation Microflowns (possibly germanium types) will meet those demands.

The application as a high-end microphone is in first instance out of reach. However, certain applications in this field are developed. Because pressure gradient microphones are not very sensitive for low frequency sound waves (and Microflowns quite good at lower frequencies) a combination of a Microflown and a pressure gradient microphone is realised to create a high-end wide band velocity microphone-pair with a figure of eight polar pattern. Such “two-way” microphone system could be used for recording purposes, see chapter “D”.

Another noise reducing possibility is to increase the effective length and thus power dissipation of a Microflown by a factor 100. A so-called Megaflown has considerable lower noise figures and can be used as a high-end microphone for studio recording purposes, see chapter “D”.

The use of a Microflown as a measurement microphone is a very suitable application because of its unique capability to measure particle velocity. Not only the Microflown itself are developed in such way that it is a reliable device, also the packaging, preamplifiers and calibration possibilities are developed in such way that it is “plug and play”.

Generator versus modulator type sensor

Although the Microflown is capable of generating sound, it is still a modulator type of sensor. This is because the way that sound is transduced in electrical signal is completely different than the way electricity is converted to sound.

Electricity is heating both wires of the Microflown and particle velocity is altering the temperature distribution around these wires. The temperature difference is the output so the sound wave is varying an

energy flow. No acoustic energy is converted in to electrical energy. If the Microflown is used to produce sound, a varying electrical power is put in both wires (or in one of the wires). Due to varying electrical power the wires will vary in temperature and these temperature variations generate sound.

A loudspeaker converts electrical power in acoustical power. This process is reversible: A loudspeaker can be used as a microphone and a microphone can be used as a loudspeaker.

Materials choice/production technique

The Microflown has a silicon based production technique, which makes it possible to integrate a Microflown on a chip. There are microphones available that are made at a similar method. However it takes more process steps and different processes to make silicon based microphones, the silicon microphones are therefore not cost effective. The size microphones will not decrease dramatically due to the silicon production technique.

Selfnoise / signal to noise ratio

The selfnoise is the electrical output of a microphone caused by internal noise of the expressed in a sound level. The air layer in the air gap causes this (thermal) noise of a condenser microphone. For lower frequencies the preamplifier (1/f) noise will dominate. If the microphone will be used for speech purposes the noise will be given in dB(A) and if it is used for sound measurements, noise measured in a narrow band is preferred.

Table 1: Selfnoise of various microphones in dB(A)

Low cost	Miniature	High end P	High end PG	Measure
34±2	27	12	17	20

The half-inch measurement microphone GRAS Type 40AC has been compared to the half-inch ICP Microflown this microphone has a selfnoise of 27dB(A).

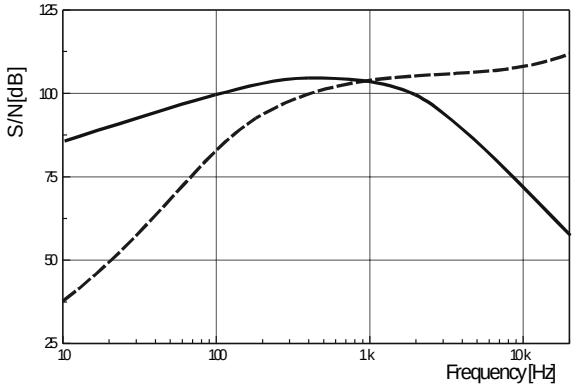

Fig. 41: Measured signal to noise ratio of a GRAS Type 40AC (½" Free field): dotted line Noise is in V/√Hz. Signal (14mV/Pa) is calibrated only at 1kHz and is assumed to have a flat frequency response. Solid line is the signal to noise ratio of a ½" ICP probe.

Bandwidth

The bandwidth is defined as the range of frequencies within a microphone delivers a usable output signal. A microphone can be considered as a mass-spring system. Such systems can not be used above its resonant frequency since the sensitivity drops dramatically. At the resonant frequency itself the sensitivity varies several dB.

Table 2: bandwidth of various microphones in kHz				
Low cost	Miniature	High end P	High end PG	Measure
0.1-7	0.05-20	0.01-20	0.25-17k	0.001-20

The output signal of a Microflown can be used up to 20kHz. The selfnoise however will be unacceptable for sound recording purposes. For speech purposes like the telecom application the selfnoise is acceptable (30-35dB(A)). For measurements (using a ½" ICP Microflown) the signal to noise ratio is good enough, sound levels can be measured (in 1Hz bandwidth) well below the threshold of hearing. Technically speaking the bandwidth of a Microflown is very high because the output of a Microflown is linear up to very high frequencies (only the sensitivity drops).

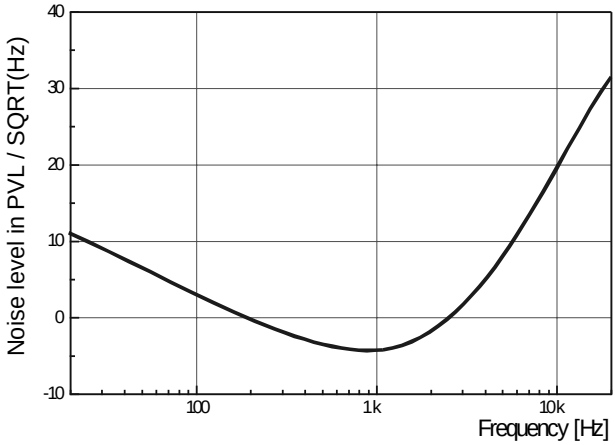

Fig. 42: Measured noise level of a ½” ICP probe in dB PVL per square root Hertz.

Upper sound limit

If a microphone is used above the upper sound limit the electrical output of the microphone will not be in linear relation with the sound pressure anymore. The due to non linear electronics the upper sound limit for a ½” ICP probe is about 100dB PVL. For other preamplifiers this limit is not determined yet.

Table 3: Upper sound pressure limit in dB SPL				
Low cost	Miniature	High end P	High end PG	Measure
95	100	140	140	150

Sensitivity

The **sensitivity** is given as the microphone's electrical output caused by a sound pressure and is noted in Volts per Pascal.

The sensitivity of a Microflown is given in Volts per 2.2mm/s. This seems to be a strange reference however in a plane wave 1Pa sound pressure will cause the particle velocity to be 2.2mm/s. The 2.2mm/s is denoted as 1Pa*. So if a microphone has a sensitivity *x* mV/Pa and the sensitivity of a Microflown is *x* mV/Pa* then in a plane wave the output will be the same; so 1Pa*=1[m/s]/ρc.

Polar pattern

A polar pattern (or microphone directivity) expresses the sensitivity to the angle of incidence of the sound field. A sound pressure microphone should be omni-directional which implies a constant sensitivity for any angle of incidence of the sound field. The larger the membrane radius (and thus physical size) the more the microphone behaves as an obstacle in the sound field. Due to this effect the directivity of the microphone increases for higher frequencies. Another cause of directivity of sound pressure microphones is related to the diameter. When the wavelength is becoming smaller than the diameter, and the angle of incidence sound wave is not perpendicular to the membrane, one part of the membrane is puled and another part is pushed. The sensitivity will be reduced due to this phenomenon.

In normal use the Microflown has a figure of eight polar patter, see Fig. 25. The Microflown can be packaged in such way that the polar pattern will be omni-directional, see chapter D1: “the sound pressure Microflown”.

Power dissipation

The capacitive pressure microphone itself does have very low power dissipation, however the use of a preamplifier is required and this will increase the power dissipation.

The power dissipation of the miniature microphone is 0.3mW. This is at a operating power of 1.5V.

The high-end audio microphone uses normally a Phantom powering (48 volts P48 provided through 6.8k resistors, see further DIII “*Add-on Microflown for a high end pressure gradient microphone*”). If the microphone is operated with phantom powering, the power dissipation is in the order of 200mW. The power dissipation of a Microflown that is Phantom powered is the same.

Stability

The stability (of sensitivity) of measurement and studio microphones is very high. Low cost microphones can vary several dB with temperature and time. No research efforts are spent yet to investigate the stability of Microflown.

A7 THE U^2 PROBE

In many applications a miniature, high signal to noise ratio sound probe is required. The signal to noise ratio of a “naked” Microflown is not very high. Due to proper packaging, the signal to noise ratio increases 10-15dB and this elevated ratio is satisfactory for many applications. The unavoidable downside of this way of packaging the enlarged size. Therefore another way enhancing the signal to noise ratio without enlarging the total device is sought for. The method that is presented here consists on two sensitive Microflowns of which the cross-spectrum will be the output, it will be therefore be called the u^2 probe.

The concept

To enhance the signal to noise ratio, a system of two non-packaged Microflowns will be constructed in such way that the total physical dimensions will not exceed 5mm in width. The cross-spectrum will be taken from the output of the two Microflowns. Due to this the signal to noise ratio will increase. This is because the cross-spectrum of the noise spectra of both Microflowns is theoretically zero (the noise spectra are non-correlated). Preliminary measurements showed an improvement of 10dB. A similar method (utilising two microphones in stead of microphones) is successfully utilised by OH Bjor, Measurement of extremely low sound pressure levels, inter-noise 97 Budapest pp. 1367-1370.

Measurements

The noise spectra of the u^2 probe have been measured. The sensor resistance value equals 1kΩ and a constant voltage circuit was used. On the basis of thermal noise theory one should expect a noise output voltage of the Microflown of (see chapter 4):

$$\delta u = \sqrt{4kTR} = \sqrt{4 \cdot 1.38 \cdot 10^{-23} \cdot 600 \cdot 500} = 4nV / \sqrt{Hz} \qquad (114)$$

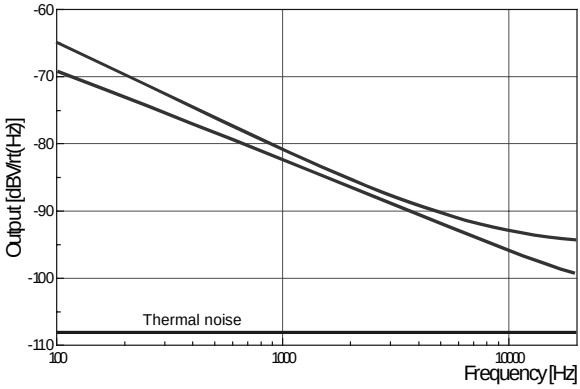

Fig. 43: 61.2dB amplified noise spectrum of the individual Microflowns of the u^2 probe.

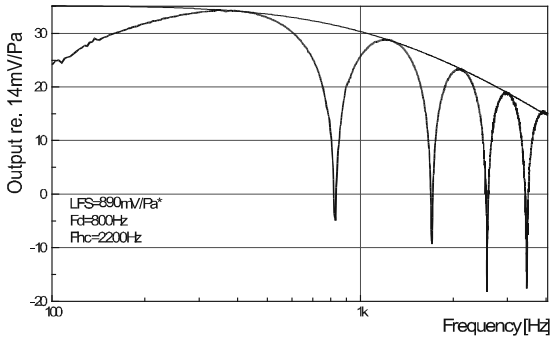

Fig. 44: 61.2dB amplified calibration measurement in a standing wave tube of the individual Microflowns of the u^2 probe.

Calibration measurements (see above) show that the (61.2dB amplified) sensitivity of the individual Microflowns of the u^2 probe is given by:

$$Output = \frac{890mV}{\sqrt{\left(1+\left(\frac{f}{880}\right)^2\right)\left(1+\left(\frac{f}{2200}\right)^2\right)}} \tag{115}$$

The u^2 probe

The low frequency sensitivity of the 61.2dB amplified Microflowns is 890mV or –1dBV. The low frequency signal to noise ratio without 1/f noise would be in the order of 100dB/√Hz.

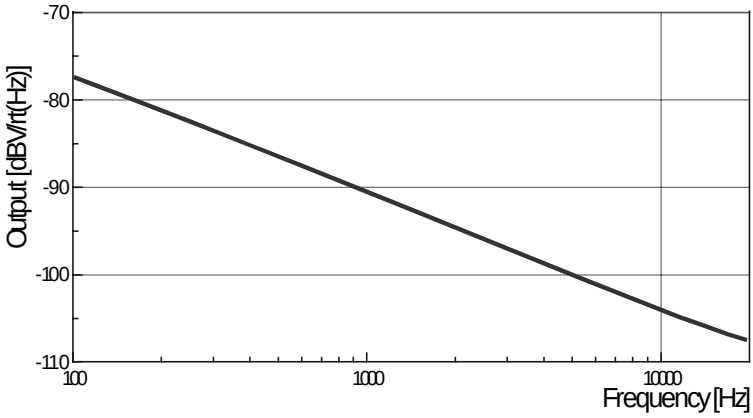

Fig. 45: 61.2dB amplified noise spectrum of the u^2 probe: noise level is about 10dB lower than the auto spectrum noise spectrum of the individual Microflowns.

Fig. 46: A realisation of the u^2 probe.

The u^2 probe